THE ASTRONOMICAL JOURNAL VOLUME 109, NUMBER 1 JANUARY 1995

THE OPTICAL AND NEAR-INFRARED COLORS OF GALAXIES. II. SPECTRAL CLASSIFICATION[1]

MATTHEW A. BERSHADY[2,3]

Department of Astronomy and Astrophysics, The University of Chicago, 5640 S. Ellis Ave., Chicago, Illinois 60637 and University of California Observatories/Lick Observatory, University of California, Santa Cruz, California 95064

Electronic mail: mab@lick.ucsc.edu

Received 1994 July 11

ABSTRACT

We have used optical and near-infrared photometry of a well defined sample of field galaxies with spectroscopic redshifts [Bershady *et al.*, 108, 870 (1994)] to study and characterize the trends and dispersions of rest-frame colors at intermediate redshifts of $z \leqslant 0.3$. We have constructed a simple spectral synthesis model which serves to determine the information available in our five bands (U, J, F, N, and K) to constrain the stellar composition of galaxies, as well as to classify spectrally our sample. We find that a simple model consisting of two stellar spectral types can reproduce well the observed broadband colors, but only if the types are allowed to vary. The five primary galaxy spectral types resulting from this model are bk, bm, am, fm, and gm (lower-case letters refer to stellar types B, K, etc.), and are distinct both in stellar type and mixture. The hottest galaxy spectral types have a very narrow range of stellar fractions, whereas the cooler types show a broader range of stellar fractions that are qualitatively consistent with more sophisticated stellar population synthesis models of similar stellar systems. Two types, am and fm, have similar rest-frame colors, although am-type galaxies are on average 2.5 times more luminous. We describe how our spectral synthesis model, when fit to the observed colors of galaxies, provides an accurate interpolative means for determining rest-frame colors. The κ-corrections calculated in this way are consistent with more sophisticated models and observed spectral energy distributions of local galaxies. Spectral classification is well suited for the study of distant galaxies because of the direct connection between spectral type and κ-correction. κ-corrections for the K band, however, are shown to be very uniform for all galaxy types to $z = 0.3$, as predicted by models. The mean K band κ-corrections are tabulated as a function of redshift. Luminosities in all bands are also tabulated for individual galaxies. The rest-frame color distributions of our galaxies are comparable in range to local samples; there are no new spectral types at the intermediate redshifts and magnitude limits of our sample. In the $U-V$, $V-K$ two-color plane, the trend of the rest-frame colors with galaxy spectral type well matches the mean distribution of local galaxies binned by morphological type. Particular attention is paid, however, to the scatter in these colors. Color–luminosity effects are observed in both $V-K$ *and* $U-V$ for *all* galaxy types over a combined range of 10 magnitudes. The range of colors at a fixed absolute magnitude is comparable to the change in mean color over the observed absolute magnitude range. In contrast to studies of galaxies segregated by Hubble type, we find no evidence for a strong galaxy *spectral* type dependence on the slope of the color–luminosity correlation. If physical parameters, such as age and metallicity give rise to the relationship between color and luminosity, they must conspire to produce similar effects for all galaxy spectral types.

1. INTRODUCTION

In 1957 Morgan and Mayall established that a strong relationship existed between galaxy spectral type, as defined spectroscopically in the same ways as for stars (the Yerkes MK system), and morphological characteristics, such as the degree of central concentration of light. Effectively, they showed that an approach to galaxy classification that begins with the characteristics of the spectral energy distribution and then correlates these attributes to morphological indices was viable. This is in contradistinction to Hubble's classification scheme (Hubble 1936; Sandage 1961), which essentially has evolved from the opposite direction: Hubble's morphological types were subsequently found to correlate with color (see Whitford 1975 for a review, or de Vaucouleurs *et al.* 1976).

However, as noted by Searle *et al.* (1973 and references therein), there are often large variations in color for galaxies similarly classified on the basis of their morphology, particularly for the "latest" types, as defined in the Hubble or other morphological systems. Huchra (1977) illustrates the large variation in $U-B$, $B-V$ color for *all* Hubble types: The dispersion in color within each Hubble type is larger than the mean difference in color between Hubble types. There are also large variations in other fundamental physical attributes

[1]Submitted in partial fulfillment of the requirements for the degree of Doctor of Philosophy, The University of Chicago.

[2]Visiting Astronomer, Kitt Peak National Observatory, National Optical Astronomy Observatories, which is operated by the Association of Universities for Research in Astronomy, Incorporated, under cooperative agreement with the National Science Foundation.

[3]Hubble Fellow.

 0004-6256/95/109(1)/87/34/$0.90

within each Hubble type, most notably luminosity. This prompted van den Bergh, for example, to develop the system of luminosity classes (1960a, b), later adopted into the Hubble scheme by Sandage and Tammann, as presented in the Revised Shapley-Ames Catalogue (RSA 1981). Nonetheless, as noted and illustrated in the RSA, correlations between morphology and luminosity are indeterminable within factors of 10 in luminosity.

The dispersions in galaxy properties within each Hubble type alone are not alarming, but what is problematic is the lack of a well defined scheme for ordering these variations. One can argue that the Hubble classification is difficult to quantify objectively, and that moreover the chosen morphological indicators are not optimized to distinguish between different physical systems (Morgan 1970). From a somewhat different perspective we can ask: Are the Hubble classification parameters the most useful to constrain models of galaxies? From the standpoint of spectral energy distributions and hence stellar content, certainly they are not. For the study of distant galaxies in particular, consistent measures of morphology are difficult due to the change in apparent size and subsequent resolution as a function of redshift. On the other hand, integrated colors or spectra are tractable, quantitative measurements. Therefore a scheme like Morgan and Mayall's that begins by distinguishing on the basis of spectral properties should be particularly fruitful for classifying distant galaxies. Spectral classification is even more enticing for the study of distant galaxies because the main ingredients that determine the relative visibility of a galaxy as a function of redshift—κ-corrections,[4] image concentration, and surface-brightness—should be strongly correlated with spectral type.

Another significant conceptual achievement of Morgan & Mayall's (1957) work was to demonstrate that in the blue (λ3850 to λ4100), galaxies, which are undoubtedly composite stellar systems, could be characterized spectrally by one or at most two stellar spectral types. Aaronson (1978) developed this concept by showing that when broadband photometry is extended from the optical into the near infrared, a second stellar spectral type is required to model the mean trend of optical–near-infrared galaxy colors, but still his model remained very simple. Specifically, Aaronson found that the $U-V$, $V-K$ color distribution of local galaxies of all Hubble types could be described by an admixture of A0V and M0III stars. It is important to understand whether the simplicity of Aaronson's model is a reflection of the intrinsic stellar composition of galaxies, and therefore physically meaningful, or an artifact of the information content in his two broadband colors. As Aaronson himself pointed out, there is also significant scatter of the observed galaxy colors about his simple model predictions. Such deviations themselves contain information on the further complexity of galaxy spectral energy distributions (SEDs).

Our interest in analyzing the observed galaxy SEDs as defined by broadband photometry is motivated by the desire to understand the stellar composition of galaxies, to determine their rest-frame energy distributions, and to predict the appearance of more distant galaxies. We also seek to tag or classify galaxies by spectral type, as defined by broadband colors. This will establish a cosmologically independent referent, thereby enabling us to compare meaningfully distributions in luminosity and (in future work) morphological characteristics at different redshifts. In addition, so that we may know whether physical meaning can be attached to our spectral classification scheme, we seek to estimate what information is available in the broadband colors to decompose galaxies into their stellar constituents. Our approach to spectral classification is then to adopt the simplest model that is capable of describing the observed optical and near-infrared colors of galaxies. The parameters of this model will become the classifiers. In this paper we have followed Aaronson's approach to spectral synthesis in order to determine the simplest possible model that adequately describes the range of our observed galaxy colors (Bershady *et al.* 1994, hereafter referred to as Paper I). We have the advantage of two additional broadbands at intermediate wavelengths (effectively B and I), and therefore we can test Aaronson's model in light of this additional information. We will show that our classification, based on a model which is necessarily more complex than Aaronson's, has an intuitive physical interpretation. In the context of *spectral* classification, we will examine the trends and dispersions of colors with galaxy spectral type and luminosity, completely independent of any reference to Hubble type. We intend the remaining analysis and discussion as a prologue to future study of the relation between distant galaxy morphology and spectral type.

We present further motivation for, development, and results of the simple spectral synthesis model and classification in Sec. 2. In Sec. 3 we describe the derivation of κ-corrections for our galaxy sample, and compare the trends of these κ-corrections with redshift to predictions of more sophisticated models and observed spectral energy distributions of galaxies. We construct and tabulate rest-frame colors for our galaxy sample in Sec. 4, compare them to local samples, and describe the trends of color with galaxy spectral type. In Sec. 5 we explore color–luminosity effects in both optical and optical–near-infrared colors, and discuss our interpretation of this phenomenon in the context of spectrally classified galaxy types. Section 6 contains a summary of the specific results of this work.

2. SPECTRAL ANALYSIS AND CLASSIFICATION

Before we turn to our simple spectral synthesis model and the outcome of our classification, it is important to point out why we have not made use of published κ-corrections (observed spectra) or sophisticated photometric models of galaxies.

Spectra of galaxies covering both a wide range of types as well as wavelengths (from ultraviolet through the near infrared) do not currently exist in the literature. Spectra at optical and ultraviolet wavelengths do exist for a limited set of galaxies [e.g., Pence (1976), or more recently the optical spectra

[4]To avoid confusion with the near-infrared K band, we use κ when referring to the photometric correction accounting for the redward shifting of the spectrum due to the expansion of the Universe.

of Kennicutt (1992)], and these spectra have been extended further into the ultraviolet by Coleman *et al.* (1980). However, there is no published, comprehensive set of spectra of galaxies observed at near-infrared wavelengths. If we extend the ultraviolet and optical spectra (e.g., Pence 1976) into the near infrared via observed broadband near-infrared colors, we find they poorly fit both the observed near-ultraviolet and near-infrared colors of our galaxies. For example, if we constrain the template energy distributions using our redder bands (F, N, and K), residuals of order 0.5 mag (rms) exist to the fits in the U band. In the opposite case, fitting to the U, J, and F bands, the residuals in the K band are of order 0.3 mag. These residuals are considerably larger than the photometric errors. Our interpretation of this result is that the sample of galaxies used to establish the templates is not representative of *all* of our galaxies. In fairness, in extending the published optical spectra into the near-infrared, systematics may have been introduced because we had to make some assumptions about the photometric systems used to define the broadband colors. We have chosen to use both the observed and model $V-K$ colors tabulated by Yoshii & Takahara (1988). However, we suspect that this is not entirely the problem. Considering that Pence used at most six galaxies to span the entire spiral sequence, any combination of effects of metallicity (correlating with luminosity) or episodic star formation (see, for example, Larson & Tinsley 1978, and Struck-Marcell & Tinsley 1978) will be poorly sampled.

In contrast, detailed galaxy spectral synthesis models do have sufficient flexibility to fit our galaxy SEDs. Quite the opposite, the problem is that the high level of sophistication in the current models is daunting, and a degree of degeneracy in the predicted colors exists between models using different sets of input parameters and ingredients. Consider the incredible power and complexity of the state-of-the-art population synthesis model. As was the case for earlier models (see Tinsley 1980 for a review) the current models require a set of stellar evolutionary tracks, a stellar mass function, and a star formation rate in order to set up a grid of stars as a function of mass, stellar age, and cosmic time on the theoretical HR diagram. To this must be mapped a spectral library, constructed either observationally or via model stellar atmospheres, or both. Recent developments have fallen into three rough categories. In one category, model makers have concentrated on improving the stellar tracks and completeness of stellar libraries, (e.g., Guiderdoni & Rocca-Volmerange 1987; Charlot & Bruzual 1991; Rocca-Volmerange 1992; Bruzual & Charlot 1993, hereafter referred to as BC93). In a second category, the effects of chemical evolution have been included and assiduously explored (Arimoto & Yoshii 1986, 1987; Arimoto *et al.* 1992; Mazzei *et al.* 1992). Finally, Renzini & Buzzoni (1986) and Buzzoni (1989) have explored models which pay strict attention to the Fuel Consumption Theorem (Renzini 1981). Many of these models include the effects of internal extinction due to dust. Comparison of various models can be found in BC93 and Mazzei *et al.* (1992). Although this list of efforts is incomplete, the point is that the variety, and complexity of the models is considerable, as is the attention of the model makers to the critical parameters and ingredients.

From a theoretical perspective, the best understood model ingredient is the stellar evolutionary tracks that are based on calculations of stellar interiors. However, all of the details of stellar interiors are not ironed out, as indicated by the recent debate between Maeder and Chiosi (see the proceedings of IAU Symposium No. 149). In comparison, our knowledge of the detailed history of the star formation rate and the mass function for external galaxies is woefully inadequate. Kennicutt (1983) has shown that current massive star formation rates in galaxies can be estimated, and that the ratio of current to past average rates also can be constrained well by broadband colors (assuming some time-invariant initial mass function). But the detailed temporal variations in the star formation rate of galaxies is not well determined. To proceed, model makers have necessarily relied either on empirical results from the solar neighborhood (for the mass function), or simplicity arguments to invoke smoothly changing star formation rates as a function of time that match the present-day colors of galaxies *assuming* a galaxy age of 10 to 15 Gyr. Larson & Tinsley's work (1978) points out that smooth star formation rates are not necessarily a valid assumption for all galaxies, even from a modeling perspective. To add to these uncertainties, the effects of dust on the integrated colors of galaxies is unknown.

We also know that stellar libraries are likely to be incomplete, in particular for stars of nonsolar metallicity. This is potentially a serious problem. For example, super-metal-rich stars may be important in understanding the integrated light in the near-infrared in bulge dominated systems, and low metallicity stars must no doubt dominate the integrated light in the youngest systems. Model stellar atmospheres are very useful for extending our observed list of spectral types (see discussion in BC93), although for the coolest stars, the complexity of the molecules in the atmospheres makes the calculations very difficult. However, broadband photometric data can be used to supplement the libraries for the coolest stars (see Frogel 1988 for a review). Since such considerable effort has been made to compile spectral libraries, it is important to test whether we have the information to discern any library incompleteness.

Our approach here is to obviate any assumptions about the theoretically poorly constrained and observationally unknown model parameters. Instead, we explore what we can learn from galaxy colors about the basic stellar composition of galaxy SEDs. With regard to the galaxy models, here we simply hope to learn what the models must be able minimally to reproduce, and hence what constraints can reasonably be expected from broad-band data. Specifically, we also test the completeness of the stellar library of BC93. The simple models we will construct include neither the effects of dust nor metallicity (note that BC93 have culled a library of roughly solar metallicity). Such effects will undoubtedly effect the colors of galaxies, but as long as our simple models can fit the observed colors, these effects are important only for the physical interpretation of the spectral classification.

2.1 A Simple Spectral Synthesis Model

To develop an intuition for building a simple model of galaxy SEDs, first recall that based on low-resolution spectroscopy in the blue–violet region between λ3850 and λ4100, Morgan & Mayall (1957) found that spectral types similar to stellar A through K existed for galaxies in their sample. Aaronson (1978) proposed that to lowest order, a simple model of two stars, namely A0V plus M0III, combined in various proportions, could reproduce the range of galaxy colors. He demonstrated that this was true in the $U-V$ and $V-K$ two-color plane (hereafter the *UVK* plane) for his galaxy sample covering a large range in Hubble type. We reinvestigate this result below, bringing to bear the added resolution of two additional bands, namely J and N, or effectively B and I.

Both the works of Morgan and Mayall and Aaronson imply that even if galaxies are highly composite stellar systems, their integrated light can be represented by one or two primary stellar types. (Note that Morgan and Mayall's data had the advantage of resolution higher than broadband data, but their spectra lacked the wavelength range of Aaronson's colors. In this sense these studies are complementary.) There is a particularly intuitive appeal to Aaronson's model based on what we know about stellar luminosities and effective temperatures, namely that galaxies can be characterized by a mix of representative, luminous hot and cool stars, each of which dominates the blue–violet and near-infrared region of the spectrum, respectively. At the same time, the *observed* range of spectral types from A to K in the blue–violet from Morgan and Mayall's work also has intuitive appeal since we know that star clusters have different turnoff masses as a function of age, and that beyond a certain age (mass), the red and horizontal giant branches dominate the integrated light of the cluster. We might expect that galaxies will effectively display a similar phenomenon, due either to differences in age, star formation rate, or both, even though they are not necessarily composed of a single generation of stars.

The viability of a relatively simple picture of the composition of galaxy SEDs is supported by the frequency of spectral types as seen in the solar neighborhood from the Michigan Star Catalogue (Houk & Fuentes-Williams 1982), as presented by Kron (1982, Fig. 1). Kron points out that this is a good approximation for what would be seen by an observer outside the Milky Way looking back at the solar neighborhood. What is striking is that essentially three stellar types totally dominate the integrated light: A0V, F5V, and K0III. However, would it be possible to distinguish the light of the intermediate color F5V stars from an appropriate admixture of A0V and K0III stars on the basis of broadband photometry? If so, models of galaxy SEDs need three major stellar components. Given the variety of galaxy types (colors), more than three stellar components might be needed. For example, Frogel (1985) has performed a numerical analysis of *UBVJHK* colors and CO and H_2O indices for the nuclei of late-type spiral galaxies. He has found that there is no correlation between the blue-optical and near-infrared colors, and that the integrated light must be due to a highly composite stellar population.

Additional near-infrared observations of star clusters and early-type galaxies show that the slope of the SEDs of these stellar systems is not the same even at 2 μm: Frogel and collaborators (Frogel *et al.* 1978b; Aaronson *et al.* 1978; and Frogel *et al.* 1980) find that metallicity correlates with near-infrared colors, presumably due to changes in the opacity in giant star atmospheres, which would consequently effect the radii and hence the effective temperatures of their photospheres (Bothun *et al.* 1984). Given all of the above observations, perhaps some flexibility in the choice of both hot and cool spectral types is a desirable feature to add to a simple model, in addition to the fractional contribution of the spectral types. However, such extra degrees of freedom must be warranted given the observational constraints if we are to hope that the model parameters will have any physical significance.

To determine the complexity needed to accurately reproduce *our* observed broadbands colors of galaxies, we have constructed a minimal spectral synthesis model based on the stellar spectral library of BC93 discussed in Paper I. In the context of this simple model, we have explored the need to add various degrees of freedom, namely more stellar types and/or choice of spectral type for a fixed number of types.

2.1.1 The observed color distribution and Aaronson's model

In Fig. 1 we have plotted three possible observed multicolor distributions for our galaxy sample. (These color diagrams will be referred to as *UJF*, *JFN*, and *FNK*.) The galaxies are divided into four redshift bins to separate the effects of redshift from the intrinsic dispersion of rest-frame galaxy colors. The stellar loci of the main-sequence and giant stars of the BC93 library are also plotted, appropriately shifted to the mean redshift of each bin. Our choice of colors is designed to explore systematically the range of shapes of the SEDs in different wavelength regions. Colors covering a small range in wavelength are better than colors spanning a broad wavelength baseline for separating stellar components at similar effective temperatures. This separation is most effective for temperatures producing peak fluxes in the bands used to define the colors. In contrast, broad-baseline colors, such as $U-V$ and $V-K$, are very good at separating stellar components at divergent effective temperatures.

The first thing to note is that the stellar loci form diagonal sequences from blue to red in all colors, with some minor exceptions in the blue near spectral type A and in the red for very cool M giants. A consequence is that the composite light from any combination of stars will result in a color which must be to the upper right of the loci. As such, the loci form a hard boundary, beyond which observed colors are inaccessible to *any* synthesis model using this spectral library.

In Paper I we have already considered the galaxies which have the most extreme colors. Study of Fig. 1 reveals that almost all galaxies do in fact lie to the upper right of the loci within their photometric errors (1σ). Two that do not will be discussed in a moment. First note that the potentially most serious problem comes from some of the reddest galaxies in

the *UJF* and *JFN* diagrams which hug the locus. The galaxies that are in fact beyond the locus boundary are there for a combination of determinable reasons. The effects of the finite redshift bin induces a spread in displayed colors (whereas the loci are for a single redshift), which is an artifact of our presentation. When this is taken into account, very few galaxies are in an inaccessible region of color space. Of those few, namely ones that lie parallel and just to the left of the stellar locus in the *JFN* diagram for $0.085<z<0.17$, all suffer from some degree of photographic saturation. However, their corrected colors in Fig. 1 are within 1σ of the stellar locus.

Of the two objects that lie significantly ($>1\sigma$) below the stellar locus, the first, sa57.7872, is most problematic in *UJF* ($0.085<z<0.17$), whereas its colors are within the 1σ errors for *JFN*, and it lies above the locus in *FNK*. Although this object suffers from substantial saturation in the *J* band, and therefore simply may have unreliable *UJF* colors, it is interesting to note that it lies in the one part of the *UJF* plane below the stellar locus that is accessible to composite stellar populations. This is due to the kink in the stellar locus about spectral type A mentioned above. The second object, sa57.12053, is notably below the locus in *JFN* ($0.17<z<0.255$), and is a cD galaxy discussed in Paper I.

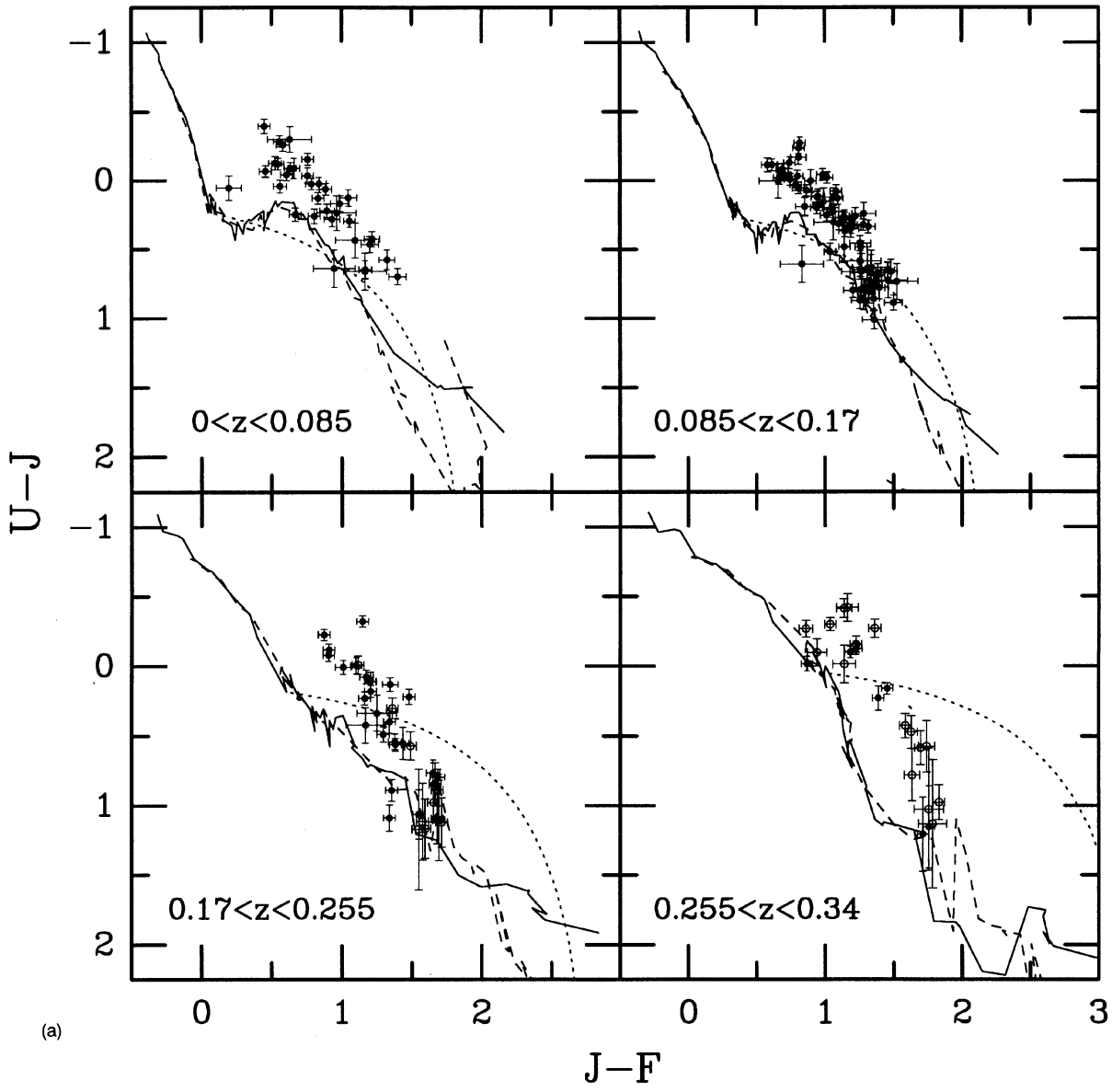

FIG. 1. The observed multicolor distribution of our galaxy sample is displayed in four bins of redshift for three different sets of colors: (a) $U-J$ vs $J-F$, (b) $J-F$ vs $F-N$, and (c) $F-N$ vs $N-K$. Filled circles represent galaxies in the magnitude-limited sample; open circles represent galaxies in the color-selected survey that are not in the magnitude-limited sample. The loci of main-sequence and giant stars from the spectral library of BC93 are shown as solid and dashed lines, respectively, redshifted to the central redshift of the bin. The dotted line represents the locus defined by all positive linear combinations of an A0V and M0III star, in analogy to Aaronson (1978), also redshifted to the central redshift of the bin.

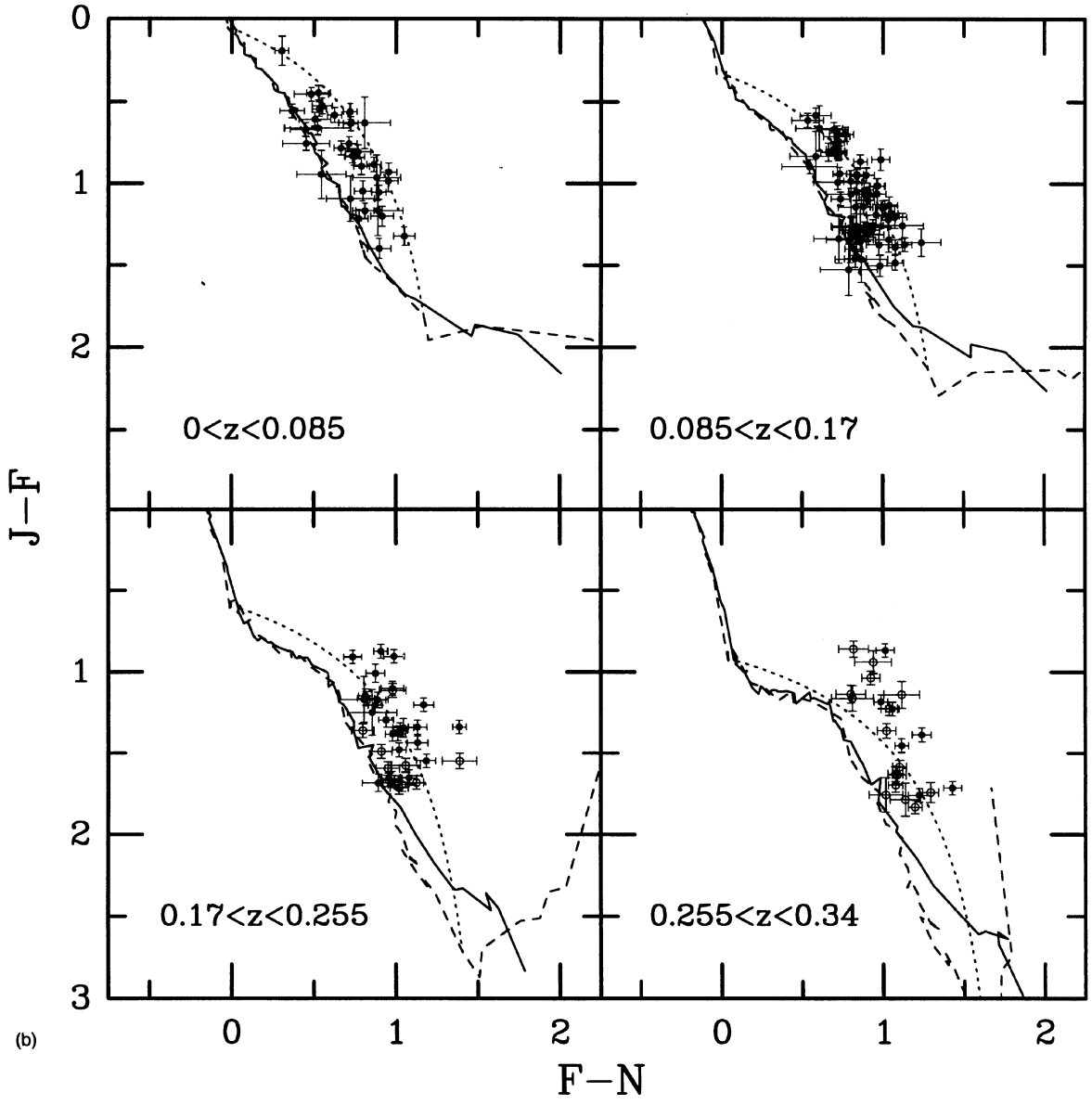

FIG. 1. (continued)

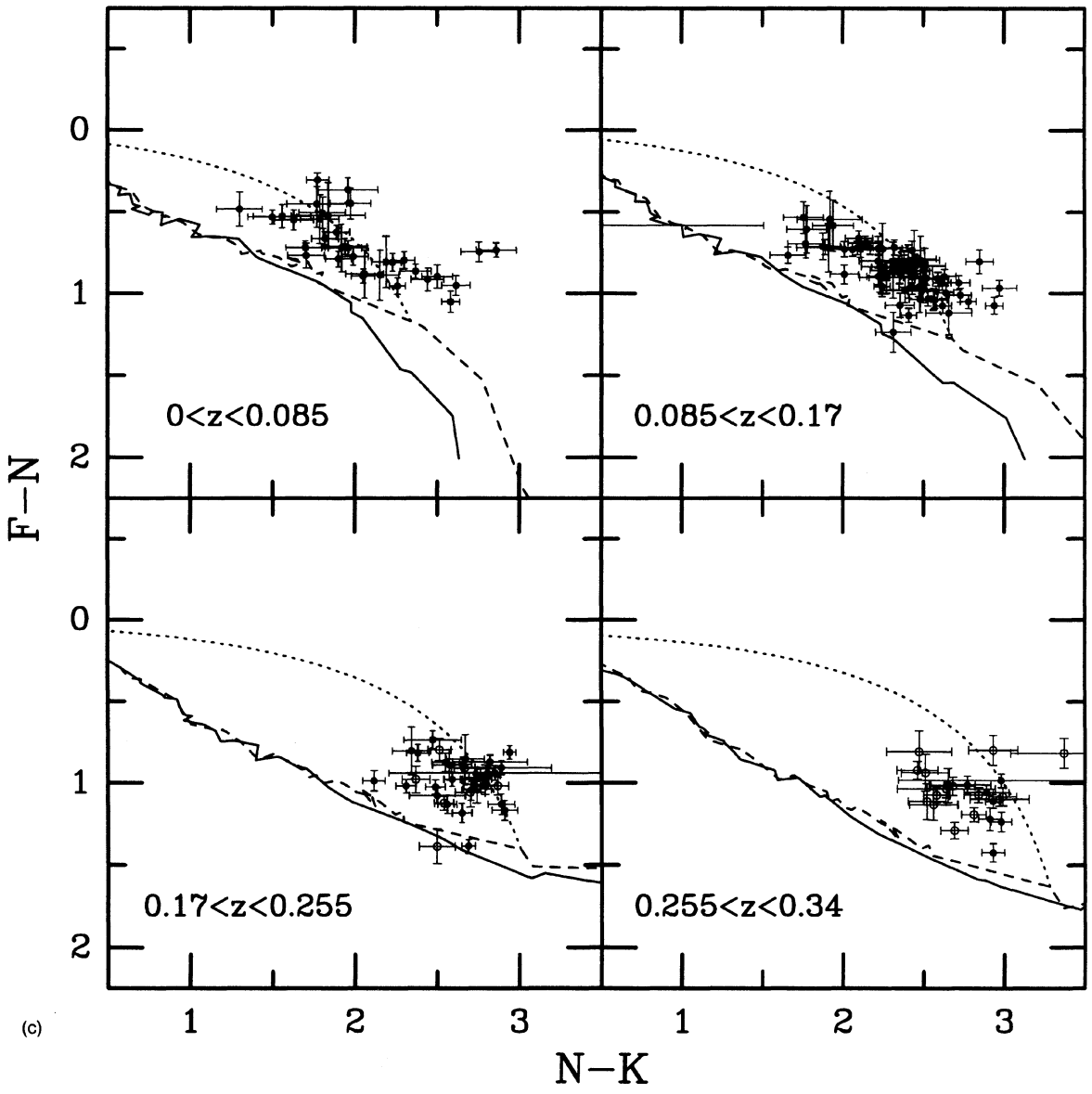

FIG. 1. (continued)

Taking all of the above into account, we can conclude that this stellar library is complete enough to span the observed range of galaxy colors. Another conclusion, based on the distance of the galaxy distribution from the stellar loci, is that *all* galaxies are clearly composite stellar systems at red-near-infrared wavelengths, namely the F, N, and K bands. To a large extent this is true at intermediate and blue-optical wavelengths, although some galaxies at these wavelengths have colors that can be represented more nearly by a single stellar type.

We have also plotted in Fig. 1 the model locus similar to Aaronson's (1978) for a linear combination of an A0V and M0III star. Here, as with the rest of our models, the stellar fraction is defined as the respective contributions of the early and late-type stars to the total F band light, in analogy to Aaronson's use of the V band. This choice is not critical, but practical given the F band's intermediate wavelength with respect to the peak flux of stars over the range of stellar effective temperatures. Note that the model *does* reproduce zero colors at zero redshift for the pure A star mix, although this is not shown in the figures. It is clear from inspection that such a simple model is unsatisfactory, particularly in the UJF plane. Although the model locus pierces the galaxy distribution in some of the color planes for some redshifts, many galaxies are either bluer or redder in all colors than this simple model predicts. We have systematically explored other combinations of two stars, but it quickly became clear that no two fixed pair of stars were adequate in any combination to span the range of observed galaxy colors.

We can infer that the success of Aaronson's model at re-

producing the locus of galaxy colors in the *UVK* plane is due to the insensitivity of the broad colors $U-V$ and $V-K$ to variations in the composition of stars dominating the blue–violet and red–near-infrared colors. This is largely because the V band light of most galaxies has significant contributions from both hot and cool stellar components. Hence, different types of hot and cool stellar components in real galaxies can be mimicked by different contributions to the V band from two, fixed hot and cool model components. In contrast, extreme colors such as $U-J$ and $N-K$ (similar to $U-B$ and $I-K$) are sensitive primarily to variations in the hot and cool stellar types, respectively. For example, while very few galaxies get bluer than $U-V=0$, a significant number of galaxies are bluer than $U-B=0$ [compare Figs. 1(a) and 13, discussed in Sec. 4.3, as well as, e.g., de Vaucouleurs *et al.* (1976), Huchra (1977), and Aaronson (1978)]. This fact indicates that stars hotter than A0 dominate the blue-ultraviolet light of some galaxies. Similarly, galaxies span a range of $N-K$ colors in Fig. 1(c) that cannot be matched by a single hot and cool star admixture (if the optical colors are also to be fit). This indicates that many galaxies are dominated in the near-infrared by stellar types earlier or later than M0. Hence the added "spectral resolution" provided by J and N bands unveils a greater range of galaxy spectral types than a simple mixture of A and M stars can reproduce.

However, note that Aaronson's model succeeds moderately well at intermediate wavelengths at higher spectral resolution, seen here in the *JFN* plane. Therefore increased spectral resolution alone is not sufficient to reveal further complexities in galaxy stellar populations, but the range of wavelengths covered is also critical.

2.1.2 Models using two to four fixed stellar types

Our next step has been to explore by trial and error just how many stars are needed to span the observed range of color space. For a fixed set of stars we find this number to be four. To see how we came to this conclusion, consider each of the color planes in turn, in Figs. 1 and 2. But first note that for any given set of stars, they may be ordered into a sequence of red to blue, for all colors (with the minor caveat mentioned above for stars near spectral type A and late M). The region of accessible color space to a model using this set of stars in *all* positive linear combinations is defined by the loci of pairs of linear combinations of stars adjacent in color (this defines the lower left boundary), and the linear combination of the reddest and bluest stars (this defines the upper right boundary). It is straightforward to see that this is true once remembering that colors are logarithms of flux ratios; the locus defined by any linear combination of two points will be more bowed the farther separated are the points.

An example of the boundaries of the available color space for four stars is illustrated in Fig. 2. The stars were chosen such that the boundaries enclose the observed galaxy distribution, duplicated from Fig. 1. The bluest galaxies in the *UJF* plane and the reddest galaxies in the *FNK* plane first dictated a hottest and coldest stellar type. The remaining two types were required in order to encompass the lower left border of the galaxy distribution in each of the three color

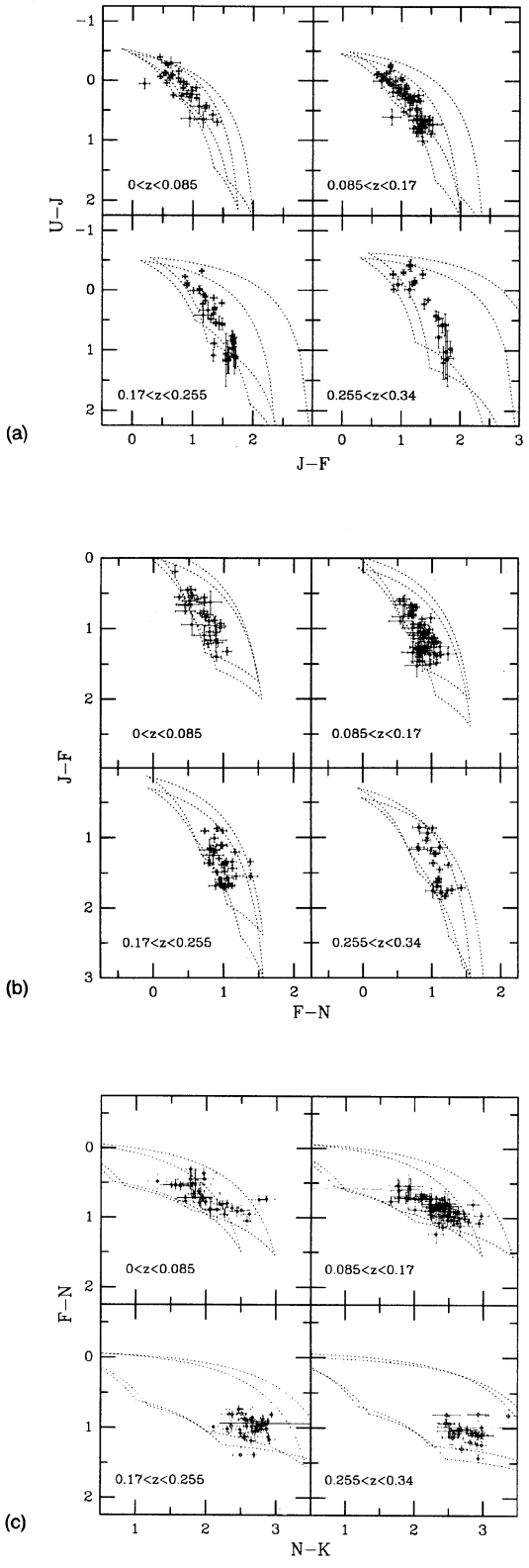

FIG. 2. The observed multicolor distribution of our galaxy sample is displayed again as in Fig. 1. Here, the dotted lines represent the boundaries of the color space attainable by all positive linear combinations of four fixed stellar types (see text): BV, G2V, K3III, M2III. The dotted lines are drawn at the redshifts corresponding to the bin boundaries.

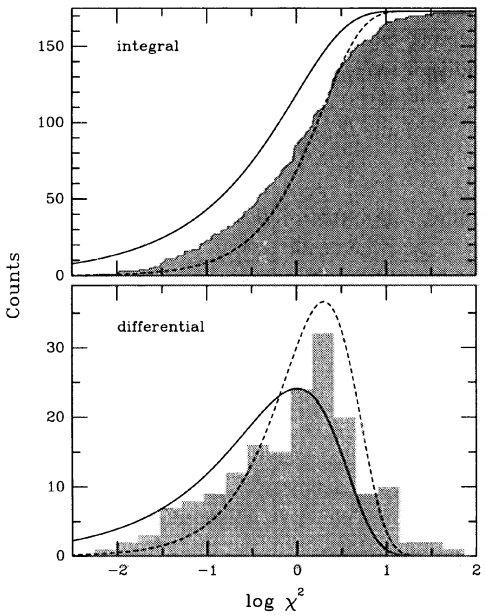

FIG. 3. The integral and differential χ^2 distributions resulting from the fits of our fixed four-star model to all galaxy colors for all galaxies. The expected distributions, assuming 1 and 2 degrees of freedom in the model, are indicated by solid and dashed lines, respectively.

planes. Our specific choices of four stars are Nos. 10, 37, 90, and 98 as listed by Gunn & Stryker (1983). The spectral types are A1V, G2V, K3III, and M2III. However, star No. 10 has the colors of a BV star, and we henceforward refer to its spectral types as such. There is nothing particularly magic about our choice; we could have used different stars of comparable spectral types in all cases.

To further test this palette of stars, we have considered a formal model for the galaxy spectral energy distribution, $g_{\rm model}$, in $N=5$ bands composed of various fractions, a, of $n=4$ stars, s, namely:

$$g_{\rm model}=\sum_{j=1}^{n} a_j s_j ,$$

where we have required the $a_j \geq 0$. The model was constructed and fit to the data in flux units, as opposed to magnitudes, so that the errors can be handled more naturally. The statistic χ^2 was defined in the usual way:

$$\chi^2=\sum_{i=1}^{N} (g_{{\rm obs},i}-g_{{\rm model},i})^2/\sigma_i^2,$$

where the σ_i are flux errors and $g_{{\rm model},i}$ and $g_{{\rm obs},i}$ are the model and observed galaxy fluxes in band i, respectively. The minimum value of χ^2 was then sought numerically.

The integral and differential distributions of χ^2 for the fits to the galaxies are shown in Fig. 3. In order to use this distribution as a diagnostic, we have been careful to consider the effects of galaxies whose photometry have large saturation corrections. A Kolmogorov–Smirnov test comparing the χ^2 distributions for galaxies with unsaturated and saturated (but corrected) optical photometry yields a 93% probability that the two are sampling the same parent distribution. (We define saturation here to mean >10% correction to any band.) Hence we have included all galaxies in our sample in Fig. 3 and in the following discussion.

We have compared the observed χ^2 distribution in Fig. 3 to that expected for a model with 1 degree of freedom, which would be true if all four stars were linearly independent in the color space spanned by *UJFNK* bands. Complete linear independence is unlikely, and indeed the observed distribution is systematically at larger values of χ^2, which is qualitatively consistent with more degrees of freedom in the model, as illustrated. However, a model with 2 degrees of freedom also does not fit well the observed distribution, both at small and large values of χ^2. Therefore it is premature to infer the dimensionality of the model, or the linear dependence of the four chosen stars. In future analysis, it would be worthwhile first to attempt to construct a basis of "eigenstars" in this color space (*UJFNK*), composed of linear combinations of stars from the BC93 or other libraries. Regardless, it is clear that the current model does not fit all galaxies as one would expect if it were a good representation of the parent distribution of galaxy SEDs.

To see this in another way, we have plotted the simulated colors for the best fitting model for each galaxy in Fig. 4. One-sided error bars in this plot indicate the magnitude and direction of the shifts of the model from the observed colors. To first order the model reproduces the mean distribution of colors, but it appears that the model is constrained to a narrower region of color space than the data, particularly in *JFN*, and to a lesser extent in *FNK*. In contrast, the residuals in *UJF* are characteristically smaller than the photometric errors. From these observations, we conclude that the model is under-constrained in the blue, and over-constrained in the red–near-infrared, or in other words that the model has too many degrees of freedom in the blue, and too few in the red–near-infrared. This may explain the χ^2 distribution which is neither consistent with 1 or 2 degrees of freedom. It is possible that a more judicious choice of four stars would produce better and more uniform results at all wavelengths, as well as a χ^2 distribution consistent with some number of degrees of freedom. We have not explored this possibility in any rigorous way.

As a final note for this class of models, we also have tried fitting all possible subsets of two and three stars from the above set of four stars. As expected, the fits deteriorated, as determined by inspecting the distributions of the modeled colors as well as χ^2. For all of the models, we do not find any correlation between the goodness of fit and redshift or apparent magnitude.

2.1.3 Models using two and three free spectral types

Although it is now clear that no two fixed pair of stars are adequate in any combination to span the range of observed colors, we have found that by fixing one type (hot or cold), and allowing both the other type as well as the stellar fractions to vary, the observed distribution in any given two-color plane can be spanned. The success of such a model requires that the fixed star be sufficiently cool or hot. How-

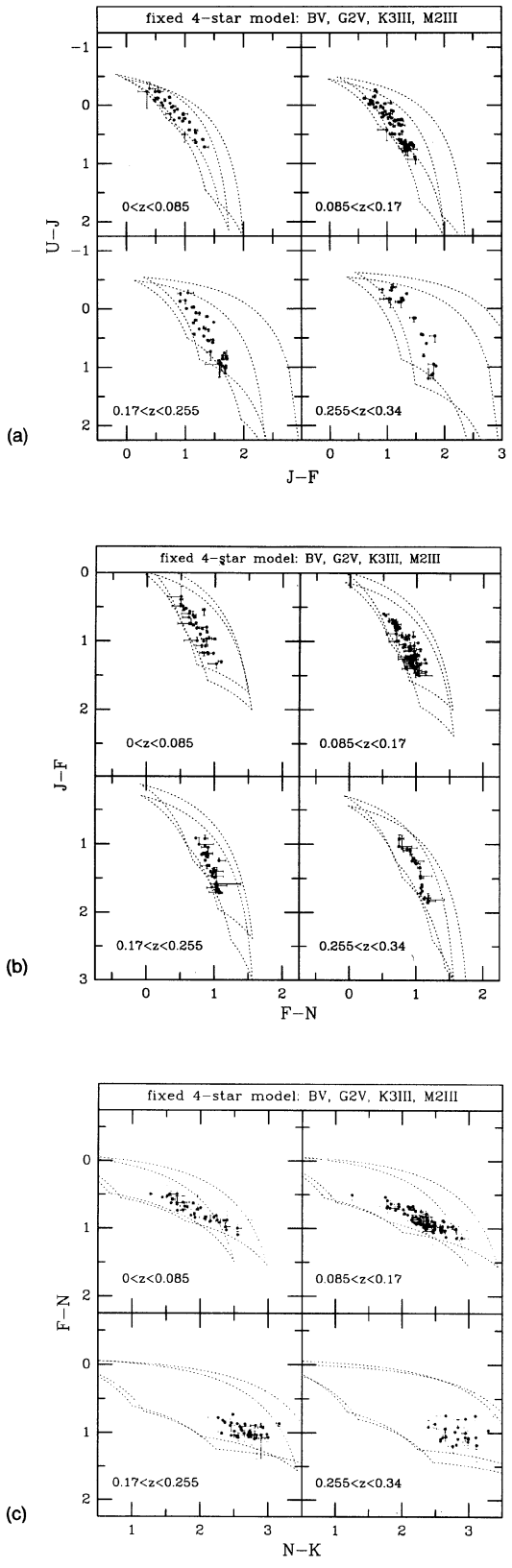

FIG. 4. The modeled distribution of colors for the fixed four-star model (see text). The colors and redshift bins are the same as Figs. 1 and 2. The dotted lines show the boundaries described in Fig. 2. The error bars represent the shift between the modeled and observed colors.

ever, there is a definite ambiguity in such an approach: Several different combinations of different pairs of stars will result in the same colors for a broad region of color space, at least for a given two-color diagram. If instead all colors are used at once, this degeneracy is largely alleviated. Remaining degeneracy can only be lifted, given the current data set, by some additional physical considerations about galaxies, such as their ages, mass functions, and star formation rates. To avoid just such considerations, we have decided not to fix any particular stellar type, since without other constraints, the choice is arbitrary. Instead, we have considered a class of models that search not only for the best combination of two stars, but also for the best pair of stars for *each* galaxy. We have considered the same type of model that include any three stars.

We discovered that about 40% of the galaxies were fitted with a cool main-sequence star (K or M), instead of giants of the corresponding effective temperature and/or type. As can be seen in Fig. 1, these two sequences have degenerate colors for all *except* the coolest stars. Based on the strength of the 2.3 μm CO band in elliptical and S0 galaxies (Frogel *et al.* 1978a, b), it is most likely that a K or M giant is the more representative cooler spectral type. To test the models including cool, dwarf stars, we will inspect the derived κ-corrections and rest-frame color distributions of our galaxies in Secs. 3 and 4. κ-corrections provide additional information about the models because they allow us to examine the slope of the model spectra about the wavelength region of each band in a convenient and statistical way. We will find that galaxies with cool, main-sequence stellar components have unexpectedly deviant near-infrared κ-corrections *and* rest-frame colors, which we take as further evidence that such stars do *not* contribute appreciably to the integrated light of galaxies in the near infrared. Therefore, for our final fits, we have imposed the added constraint that K and M dwarfs cannot be used in the two- and three-star models.[5] This eliminates stars No. 55 through 71, as listed by Gunn & Stryker (1983) (stars 70 and 71 are without matching near-infrared spectra).

To test for further degeneracy in the remaining choice of stars, we saved both the first and second-best model parameters for every galaxy. Inspection reveals that both sets were almost always of very similar spectral types, although sometimes of different luminosity classes. Typically one of the stars in the first- and second-best models was identical. Our test for degeneracy has not been more extensive than this (for example, we have not investigated the χ^2 distribution for

[5]Our finding that late-type dwarfs do not dominate the near-infrared light of galaxies is not surprising since it is consistent not only with narrowband and spectrophotometric observations but also predictions of all modern, population synthesis models. It is also not surprising that we have this discriminatory sensitivity with only our set of broadband colors. See, for example, Bessel & Brett (1988), Figs. 1–4, where they plot $V-I$, $J_{IR}-K$, $H-K$, and $J_{IR}-H$ versus $V-K$ for giant and dwarf stars, where J_{IR} refers here to the near-infrared band at 1.2 μm. For $V-K \geq 3$, a bifurcation of giants and dwarf sequences occurs in $J_{IR}-K$ and $J_{IR}-K$, but not for $V-I$ and $H-K$. From this one can deduce that such a bifurcation is likely to exist in $I-K$ (similar to $N-K$), as is seen in our Fig. 1(c). This should provide us with the leverage to discriminate dwarf versus giant star contributions to the red and near-infrared bands.

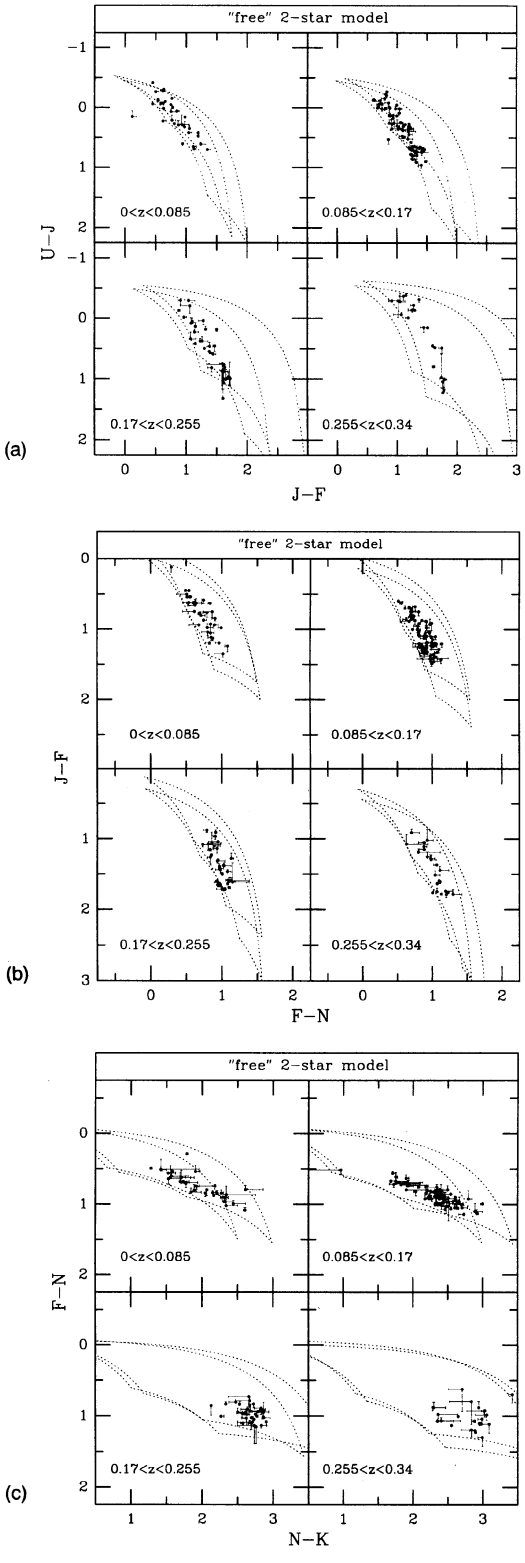

FIG. 5. The same as Fig. 4, except for the "free" two-star model.

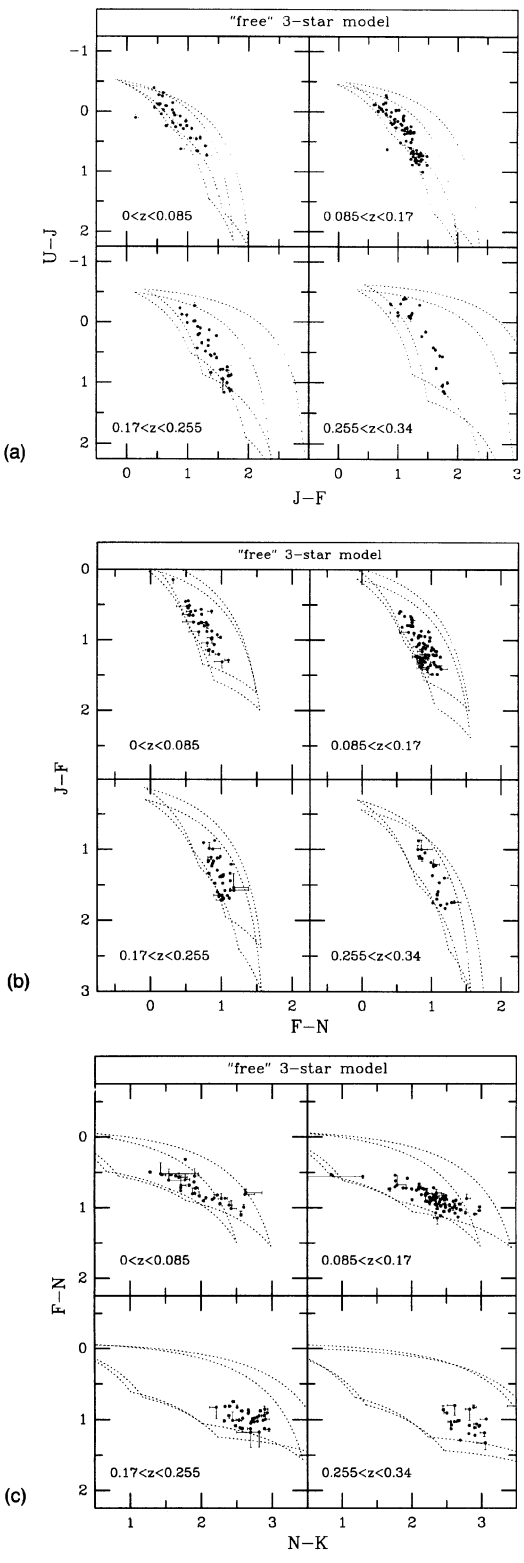

FIG. 6. The same as Fig. 4, except for the "free" three-star model.

each galaxy in the space of all possible stellar combinations), but the consistency of the classification that we will later describe reassures us that there is no serious problem in this regard.

Although χ^2 was constructed and numerically minimized in the same way as for previous models, any interpretation of the measured distribution is problematic. This is because we have not as of yet determined how many degrees of freedom

TABLE 1. The distribution of spectral types in the magnitude limited samples.

Type	Number of objects binned by fraction of F-band light contributed by cool stellar type																					
	k										k	m										m	Total
	.1	.2	.3	.4	.5	.6	.7	.8	.9	1	sub-total	.1	.2	.3	.4	.5	.6	.7	.8	.9	1	sub-total	
b	0	0	0	0	0	2	15	10	2	0	29	0	0	0	0	0	1	7	10	2	0	20	49
a	0	0	0	0	0	0	0	0	1	0	1	0	0	0	0	0	0	5	15	1	0	21	22
f	0	0	0	0	0	0	0	0	0	0	0	2	0	5	2	9	4	3	3	0	0	28	28
g	0	0	0	0	0	0	0	0	0	0	0	5	7	5	3	3	8	4	0	0	0	35	35
Total	0	0	0	0	0	2	15	10	3	0	30	7	7	10	5	12	13	19	28	3	0	104	134

have been introduced into the models by allowing for a choice of stellar type. Without a formal statistical tool to compare these "free" two- and three-star models to the fixed four-star model, we again look at the modeled color distributions. The color distribution for the "free" two- and three-star models are displayed in Figs. 5 and 6, respectively. Compared to the four-star model, both of the "free" models produce a somewhat broader color distribution that is more representative of the observed galaxy color distribution. For this reason we prefer the "free" models. We also find that the difference between the two- and three-star models is marginal, except that the shifts between the observed and two-star model colors seem most characteristic of the observational errors. Appealing to Occam's Razor, we therefore adopt the two-star model. Hence the spectral classification consists of two spectral types, and the flux ratio of these types in the rest-frame F band.

As we have indicated, to test our adopted model further, we will explore in subsequent sections the derived spectral classification, κ-corrections, and rest-frame color distributions. At each turn, we will find the results are reasonable, and that the classification has a particularly intuitive appeal. We cannot offer complete assurance at this time that this simple model is an accurate representation of galaxy SEDs, and that therefore the derived classification has physical relevance. But we suggest a robust test can be made of this two-star model by exploiting the power of the complex synthesis models described earlier: For any given complex model, replete with some choice of age, mass function, star formation rate, and scattering and extinction due to some geometric distribution of dust, find the best fitting two-star model as described here, chosen on the basis of simulated broadband colors. Inspection will reveal whether the choice of two stars is accurate given the *known* stellar ingredients of the complex model. In this way the simple model and the physical interpretation of its spectral classification can be both tested and calibrated. In turn, this will verify whether the extent of the information available in broadband colors largely consists of characterizing hot and cool stellar components.

2.2 Results of the Spectral Classification

We define the spectral classification nomenclature to consist of two lower case letters, corresponding to the hotter and cooler stellar spectral types, in that order. For example, a galaxy whose colors are modeled by some linear combination of a B star and a K star is spectrally classified as bk-type. We will sometimes refer to galaxies by a single letter from their full spectral type to call attention to either the hot or cool stellar spectral type. For clarity, when we refer to "stellar fraction," we will always refer to the fraction of the light contributed by the cooler stellar spectral type (in the *rest-frame* F band). This quantity is defined as $f_{c,F}$.

The two-star model, when fit to all of our galaxies, yields seven distinct spectral types, five of which contain most of the galaxy sample. These types are listed in Table 1, which is constructed to show the distribution of the stellar fractions for each type. The spectral types have been divided into two groups, labeled as k- and m-type, corresponding to the two coolest stellar types (K and M) found from the classification. For each of these types, the hotter stellar component runs from B through G, and hence another label b through g is chosen, accordingly.

In order to make the data in Table 1 more easily comparable to other galaxy samples, we have only included the J magnitude-limited sample, but there are no new spectral types in the color-selected sample. To define the completeness in concert with Table 2(a) from Paper I, note that the number of galaxies here total 134 instead of the 143 galaxies in the J magnitude-limited sample. The excluded galaxies consist of two galaxies without U and N photometry, and six galaxies suffering from >20% saturation in one or more bands, as indicated in Tables 6(a)–6(f) in Paper I. The ninth galaxy (sa68.13504) is interesting, however, because it has extremely blue optical colors ($J=20.5$, $F-N=0.58$, and $z=0.093$). K band photometry for this object in an aperture matched to the optical photometry is very uncertain (± 1 mag). For this reason we cannot be sure that the spectral classification is reliable, particularly for the cooler component. Nonetheless, this represents the unique galaxy in this sample classified as g-type for the cool component. The hotter component is b-type, and the stellar fraction is 0.73.

We should point out several simplifications that have been made in this representation. First, we have not differentiated between subclasses of stellar spectral type, since as of yet we cannot be certain the broadband photometry so precisely constrains the models. This may make the interpretation of the m-type galaxy spectral class problematic, since M stars exhibit a wide range in color. We will explore this in more detail in the future.

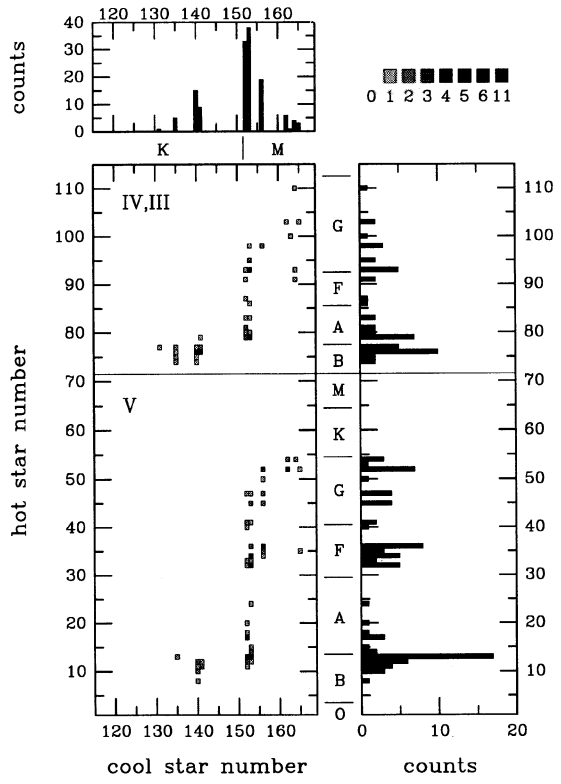

FIG. 7. The frequency distribution of pairs of stars selected by the "free" two-star model to fit the magnitude-limited galaxy sample defined in the text. The marginal distributions of hot and cool types, as defined here, are shown in the right and upper panels. The greyscale code in the upper right corner is for the main panel, and corresponds to the numbers of galaxies. The Roman numerals in the main panel denote the stellar luminosity class of the hot stars in the Gunn & Stryker (1983) atlas. The star numbers refer to the "ID" numbers therein. We have designated our spectral classification of these stars in the margins between the panels.

We have also made no attempt, either in the models or in this tabulation to differentiate between main-sequence and giant stars of the same spectral type, except as noted in the previous section for cool stars. Since the cooler component is always either k or m-type, the cooler component is always modeled by some choice of giant star.

As a diagnostic, the frequency distribution of stellar pairs selected by the model for the galaxies in Table 1 is shown in Fig. 7. The marginal distributions for hot and cool stars are also shown. This plot specifies how we have defined spectral type for stars in the Gunn–Stryker atlas. With the exception of stars 55 through 69, which we have excluded from our model (see earlier discussion concerning cool dwarfs), all the other gaps in the distribution represent the culling of BC93. Note that the distribution of stellar pairs isn't random, but displays a moderately smooth correlation, as we would hope if the model selection of stars is not dominated by noise in the data or systematics in the library. The largest spikes in the marginal distributions occur across gaps in the stellar library, most notably for the cool stars between K and M type. For this and other reasons which we will discuss below, in the future it would appear advantageous to include more stars in this omitted region. For the hot stars, the most frequently selected star is No. 13, which is at the end of our defined B dwarf sequence. Part of this "pile-up" may be due to the gap in the cool stars. However, an investigation of the stellar spectra reveals that there is a distinct change in the amplitude of the Balmer break (near 3800 Å) between stars No. 13 and 14 (see Figs. 2(a) and 2(b) in Gunn & Stryker 1983). These points serve to illustrate why we have not attempted to construct a finer grid of spectral classification.

2.2.1 Discussion

Although it is tempting to interpret this simple classification as a characterization of the prime constituents of the young and old stellar populations of galaxies, recall that this classification is as of yet uncalibrated. There are also well-known fundamental astrophysical properties of stars that make any such interpretation ambiguous. For example, the channeling of stars with a wide range of masses off of the main sequence onto essentially the same position in the HR-diagram, namely the red-giant branch, makes any assessment of the characteristic age of the cool component impossible simply on the basis of broadband colors; a mass change of a factor of two for such stars is equivalent to a change of a factor of ten in age. Without any information about the luminosity of the individual stars, it is difficult to distinguish even red super-giants—or asymptotic giant branch (AGB) stars evolved from massive progenitors—from low mass red giants. For example, determining the presence of AGB stars on the basis of extremely red near-infrared colors would require that the effects of metallicity on the red-giant branch are also somehow constrained. In contrast, the hotter spectral type can plausibly be interpreted as the effective stellar turn-off mass for the most recent episode of significant star formation in each galaxy. This interpretation is probably not valid when the hotter stellar component is as late as F or G, since horizontal branch stars may contribute significantly to the integrated light at these effective temperatures. In short, although the model may be simple, astrophysical interpretations of the model parameters are not.

We have made one simple test of our classification, namely to correlate the hotter galaxy spectral type with observed spectral emission. The results are quite favorable: In SA57 we find that of the 16 objects in our sample with emission, 10 are b-type, out of a total of 11 objects classified as b-type. The remaining 6 galaxies with emission that are types a, f, or g have equivalent widths of Hα<20 Å. In comparison, 8 of the 10 b-type galaxies that are in the redshift range to detect Hα have equivalent widths averaging around 50 Å. The equivalent width measurements are somewhat uncertain, however they serve well for this qualitative comparison.

It is interesting to remark on the gross feature of the spectral distributions in Table 1, since there are some distinct patterns. (We will explore the correlation of $f_{c,F}$ with rest-frame color in a later section.) Note that essentially all of the galaxies classified as k-type are also b-type. Further, the stellar fractions $f_{c,F}$ of b- and a-type galaxies have a very small range, with a mean value of 0.75 and a half-width of only 0.1. Is this value of $f_{c,F}$ reasonable given what we know

from sophisticated stellar population synthesis models? In Fig. 2 of BC93, the fractional contribution in the V and R bands of main sequence relative to core-helium burning stars is about 0.2:0.8 at a little under 10^7 years after a burst of star formation, for a single generation of stars. However, if this is considered a plausible explanation for the mean value of $f_{c,F}$ for b- and a-type galaxies, then the narrow range of $f_{c,F}$ requires the current rate of star formation for over 40% of our sample is sufficiently large that young, massive stars dominate the integrated light at all wavelengths of our observations.

If our model is taken seriously, the small range of $f_{c,F}$ for b- and a-type galaxies means that in physical terms the ratio of the number of hot to cool stars is very similar between these galaxies which presumably have the most active star formation. It also implies star formation rates (SFR) of massive stars per unit luminosity are very nearly the same for all of these galaxies. We have calculated the predicted massive ($\geq 10 \mathscr{M}_\odot$) star formation rates for the b-type galaxies and compared them to Kennicutt's (1983) results for late-type galaxies, and find our values are high by about a factor of 3 to 5. However, it is remarkable, given the simplicity of the model and the uncertainty in our knowledge of the initial mass function that there should be even such a close agreement. One way the two-star model could overestimate the star formation rate is if there is indeed a third stellar component contributing significantly to the F band light.

Physical interpretations of the model parameters for the cooler, fm- and gm-type galaxies are not as forthcoming. However, a very useful comparison can be made to Turnrose's (1976) stellar synthetic modeling of spectrophotometry of the nuclei of 7 Sc galaxies. First we remark that there is a dramatic change in the distribution of stellar fractions between b-, a-type galaxies and f-, g-type galaxies, namely $f_{c,F}<0.8$ for f- and g-type galaxies. The range of $f_{c,F}$ also becomes very broad for these cooler types. This is, at least partly, a result of the nonlinear relationship between effective temperature and spectral type, and our choice of the F band to represent the stellar fraction.

The galaxy nuclei of Turnrose's sample are classified in the Yerkes system as f or fg, and hence might be expected to be of similar intrinsic spectral type as fm- and gm-types in our classification. In addition, Turnrose's spectrophotometry covers the broad range from λ3300 to λ10400, and so is representative of our wavelength coverage but is at much higher resolution. Turnrose constructed what he called "constrained" as well as "unconstrained" synthetic SEDs using 34 distinct stellar spectral types. The constrained models were, in effect, similar to the current population synthesis models, since the constraints consisted of a stellar birth function that imposed continuity on the relative numbers of stars in his model. The unconstrained models are directly analogous to our "free" models. Turnrose's results are significant on several levels, and we discuss four major conclusions of his work that are relevant to our own.

First, both the constrained and unconstrained models provided comparable fractions of the same basic stellar types in the best fitting model SEDs. In some sense this was a test of Turnrose's library completeness, but also of the potential degeneracy in combining different sets of stars. Although our library and data are both different from Turnrose's, his result at least demonstrates that unconstrained models in practice get basically the right answer. Second, the stars contributing most to the integrated light fell into two groups at distinct spectral types, namely FV to GV, and KIII to MIII. Although the range of integrated spectral types of his galaxy nuclei is small, by construction, these nuclei are clearly very composite stellar systems. Therefore this second result adds further credence to the reasonableness of a simple two-star model. Third, the fraction of the light contributed by the hotter stars in the V band varied from galaxy to galaxy, but was upwards of about 50%. Hence, the distribution of $f_{c,F}$ for fm- and gm-type galaxies in our sample may be quite reasonable. Finally, some of the nuclei had clear contributions from very hot, main-sequence stars, such as O, B, and A, in addition to the F and G stars. Note that we find emission to be present in some of our fm- and gm-types galaxies. In summary, the spectral classification provided by our simple two-star model for the cooler galaxies appears to be consistent with results from at least one complex population synthesis model for comparable stellar systems.

3. DERIVED κ-CORRECTIONS

The κ-correction is the magnitude difference between a redshifted and unshifted (rest-frame) spectrum as observed through some fixed band. We adopt the definition of Oke & Sandage (1968), which is also adopted by Pence (1976). Given our multiband photometry and models there are a variety of ways we can derive κ-corrections for each band, starting by fitting a model SED to each galaxy's broadband colors:

(1) Use the fitted model SED to calculate κ-corrections using the filter response curves without any further reference to the broadband data [e.g., Eq. (1) of Pence 1976].

(2) Use the fitted model SED only to calculate the apparent magnitude in the galaxy rest frame. The κ-correction is then the difference between observed, broadband magnitude and modeled, rest-frame magnitude.

(3) Find the observed band which is closest in characteristic wavelength to the redshifted band of interest. First use the fitted model SED to derive a κ-correction between this closest observed magnitude and the band of interest, i.e., apply method (2) with the exception that the observed magnitude and modeled magnitude may correspond to different bands. (The modeled magnitude corresponds to the band of interest.) The color term between the two bands is then determined using the appropriate regions of the model spectrum. The adopted κ-correction is the sum of these two quantities.

(4) Perform the same procedure as (3), only use the two bracketing observed bands (i.e., bands observed redward and blueward of the redshifted band of interest, if available), and average the results. We have chosen to weight the average by the relative linear distance in wavelength between the redshifted band of interest and the two observed bands.

The advantage of the last two methods is that they use as

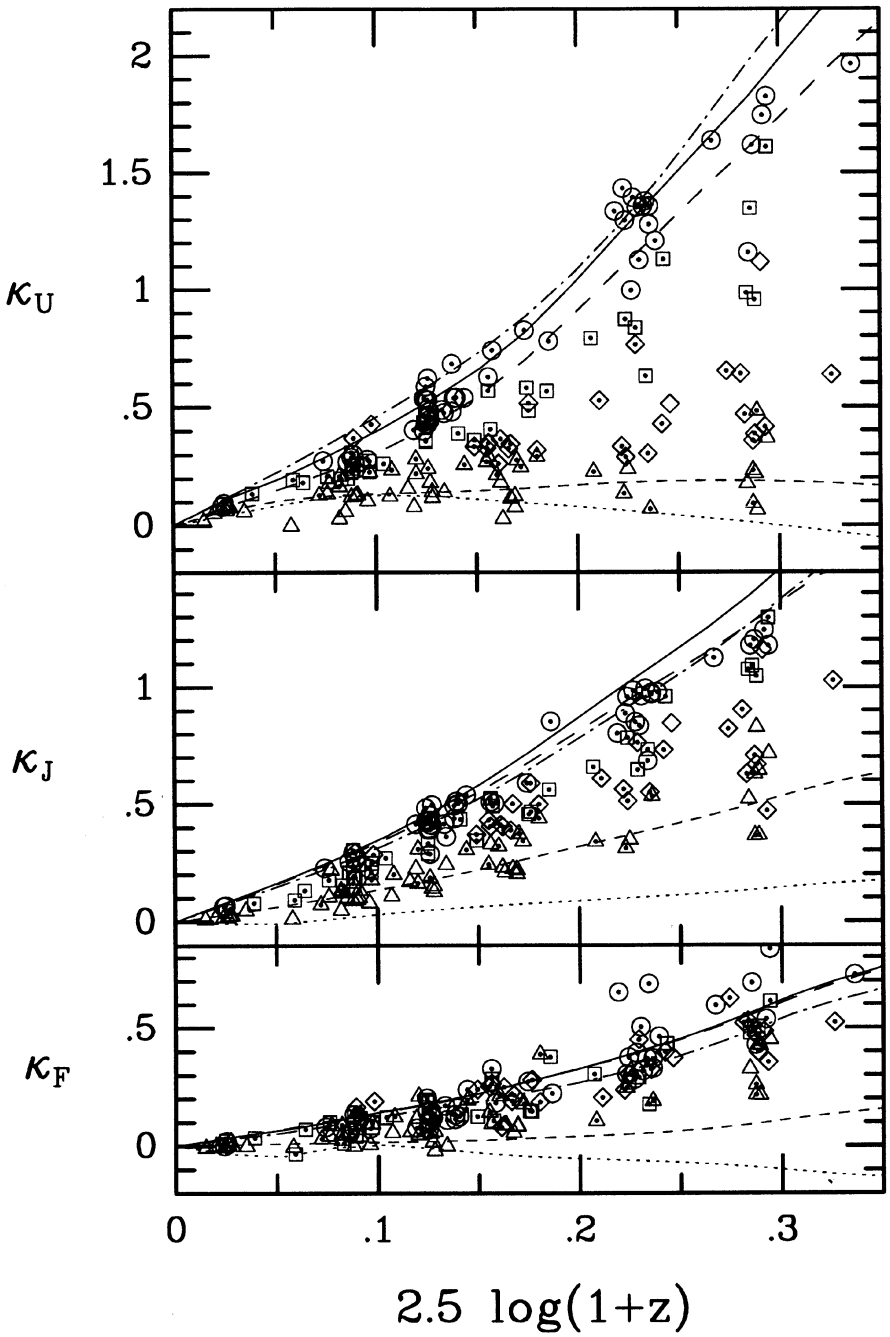

FIG. 8. The κ-corrections for the U, J, and F bands as determined from the "free" two-star model are plotted as a function of redshift. Each point represents a galaxy in our sample at its observed redshift. Galaxies with >20% saturation in any band have been excluded from the plot. Objects are marked by spectral type: b-type (triangles); a-type (diamonds); f-type (squares); g-type (circles); k-type (open); m-type (dotted). Curves represent simulations based on observed low-redshift galaxy spectra or models (BC93): the elliptical galaxy from BC93 (thin, solid line); an elliptical galaxy compiled by Persson (dot–dashed line, Bruzual 1992); 16 Gyr, single burst model (long dashed line); 16 Gyr constant star formation rate model (short dashed line); and the star-forming galaxy NGC 4449 (dotted line).

much of the observed data as possible. Moreover these methods rely on the model SEDs only to interpolate between observed magnitudes over as short a wavelength as possible, as well as to determine color terms, which are small, differential quantities weakly dependent on the model SEDs. The fourth method has the further advantage of using two instead of one observed magnitude, and these magnitudes are averaged in an optimal way. In contrast, the second and first methods rely increasingly on the model SEDs and less directly on the observed magnitudes. We have examined the results of all of the above cases. Although it is not particularly obvious when looking at the κ-corrections themselves,

the corresponding rest-frame multicolor distributions are noticeably smoother and less noisy using the last method. Since this result agrees with our expectations, we have adopted method (4) throughout the remainder of this paper. This procedure should be more accurate than what is commonly done to estimate κ-corrections, namely method (1). In other studies, often the model or template SED is chosen on the basis of as little as one color, or even worse on the basis of some estimated Hubble type (Hubble types are known to have wide range of colors; e.g., Huchra 1977, Fig. 7). Here we are taking full advantage of the wavelength sampling and coverage of our observations as well as model SEDs that are reasonably physical and can well represent the data.

Note that we can use the above methodology to calculate colors and κ-corrections at any arbitrary redshift for each galaxy. This can be done accurately as long as (i) the simulation redshift shifts the band of interest within the range of the model SED, and (ii) the band of interest does not sample bluewards in the rest-frame than the bluest observed band samples at the simulation redshift (in this case, the observed U band). The second criterion stipulates that the simulated colors and κ-corrections are derived from interpolation based on the model SEDs, and not from extrapolation. The second criterion also is always more restrictive. Since our sample extends to $z\sim0.3$, this translates into reliable simulation limits of $z=0.3$, 0.64, 1.15, 1.8, and 6.75 for the U, J, F, N, and K bands, respectively. Indeed there is a lower redshift limit as well, but this is only for the K band. Because the behavior of the SEDs appears to be very similar and smooth in this spectral region (for $0<z<0.3$ this is between H and K, see below), it is reasonable to allow the models to extrapolate to zero redshift for the K band. The simulations at higher redshifts will be presented elsewhere.

We have considered the κ-corrections for the blue-optical bands and the red–near-infrared bands separately, since this division should largely reflect the respective wavelength regions dominated by the hot and cool stellar components in the two-star model. κ-corrections are plotted versus 2.5 log(1 $+z$) since in the approximation of an SED as a power law, $f_\nu \propto \nu^\alpha$, the κ-correction becomes

$$\kappa = -(1+\alpha)2.5\ \log(1+z),$$

and then the slope in the plots is easily related to α.

3.1 Optical κ-corrections

The κ-corrections for the U, J, and F bands for each galaxy are plotted in Fig. 8 as a function of redshift, as derived from the two-star model SEDs. Galaxies are marked by their spectral type. The spread in the κ-correction at a given redshift for a single type (b,a,f,g) represents the range of stellar fractions for that given two-star combination. Note that the hottest galaxies in the U band are almost all k-type. For reference, we have plotted model tracks from BC93 for the same set as used in Paper I, Figs. 17 and 18, namely for two extreme star-formation rates at an age of 16 Gyr. We also include simulated κ-corrections as a function of redshift based on observed spectral energy distributions of local elliptical galaxies (two averages), as well as an extreme star-forming galaxy (NGC 4449). This set (referred to as the "models") provides extrema at both the red and blue end of the expected galaxy color distributions: Although there will be some galaxies with κ-corrections larger or smaller than the models, such objects should be relatively few in number. In general the κ-corrections of the two-star model look well behaved in these bands.

There are two regions where derived κ-corrections are significantly more extreme than the reference tracks. The first is for the bk-type galaxies between $0.05<z<0.175$, which appear to have smaller κ-corrections than even NGC 4449. However, these are indeed supposed to be the bluest galaxies, and if one compares the UBV colors of NGC 4449 ($U-B=-0.3$, $B-V=0.4$) against those of local fields galaxies from the Second Reference Catalogue of Bright Galaxies (de Vaucouleurs *et al.* 1976) or normal Markarian galaxies (e.g., Huchra 1977, Fig. 2), one finds NGC 4449 is not at the most extreme, blue limit of the color distribution, particularly in $U-B$. Therefore one would expect the bluest galaxies to have κ-corrections in the U band as small as or smaller than NGC 4449. Second, there are several objects which have extremely large κ-corrections in the F band at $z>0.2$. The three most discrepant points correspond to the three objects that had the most extreme red $F-N$ colors in Fig. 18 of Paper I (sa57.7693, sa57.12053, and herc1.5110). In other words, their κ-corrections are qualitatively consistent with their colors. Likewise, the number of objects with slightly larger κ-corrections than the reddest model are consistent with the number of objects in Fig. 18 of Paper I with slightly redder $F-N$ colors than the reddest model.

We have also checked for random and systematic differences in the κ-corrections derived from the various simple models we have considered (i.e., 2, 3, and 4 stars). We find that in the J and F bands, the agreement is excellent for all models, but gets somewhat worse in the U band. (This correlates with the relative magnitude of the photometric errors in these bands.) The statistics show that in the mean the κ-corrections for different models and a given band are different by at most 0.02 mag and typically much less. The dispersion is less than 0.07 mag for all bands and a typical value is 0.04 mag. These results hold for comparisons between any of the two classes of models we previously considered, namely 2, 3, and 4 stars.

3.2 Near-Infrared κ-corrections

In Fig. 9 the κ-corrections in the N and K bands are plotted for both the two-star model that includes (right panel) and excludes (left panel) K and M dwarf stars from the selection palette. The curves represent the same models and local galaxy observations as in Fig. 8, with two additions for the K band, as discussed below. The difference between the κ-corrections for these two sets of models is striking, particularly in the N band. The models with cool dwarfs imply that there are some exceptionally red galaxies. However, the modeled color distributions in the observed frame of each galaxy (e.g. Fig. 5) are ostensibly the same in the mean

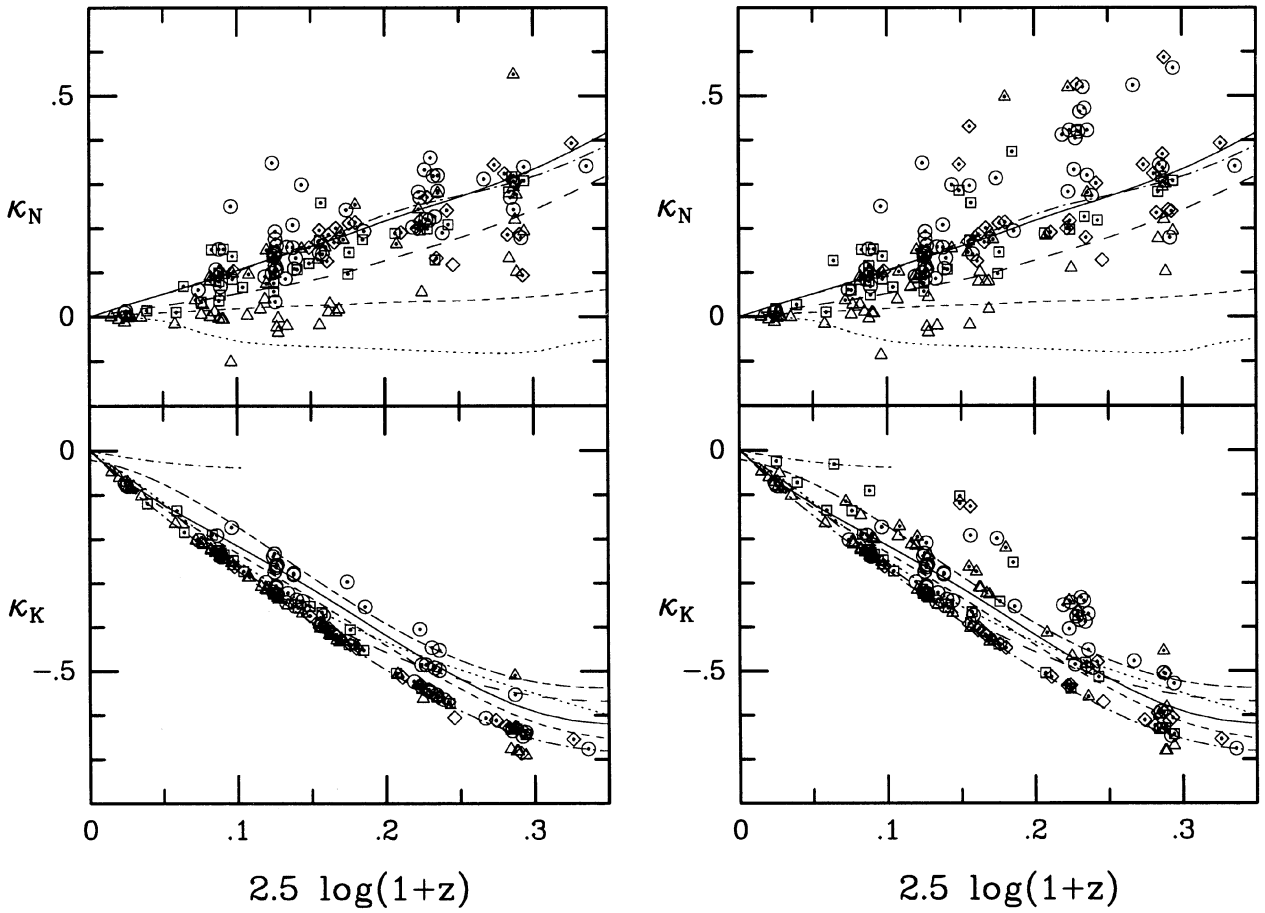

FIG. 9. The κ-corrections for the N and K bands as determined from the free two-star model are plotted as a function of redshift. Each point represents a galaxy in our sample at its observed redshift. Galaxies with >20% saturation in any band have been excluded from the plot. The left-hand panel is for the (adopted) two-star model *without* K and M dwarfs. The right-hand panel shows the effect of allowing the model to choose K and M dwarfs. The symbols and curves are the same as in Fig. 8, with the addition of two additional curves for the K band, in descending order: (1) Mobasher *et al.*'s (1986) semi-empirically derived κ-correction (small-dash–dotted line); (2) an elliptical galaxy spectrum as reported by Eisenhardt & Lebofsky (1987, long-dash–dotted line). These two curves lie above the previous four curves.

for the models with and without dwarfs, by construction. Therefore, the κ-corrections are implying that the slope of the spectra to the blue of the wavelengths sampled in the observed N and K bands are different for models dominated by dwarf and giant stars in the near infrared.

In contrast to the models with K and M dwarfs, objects with extreme κ-corrections for the two-star model without these cool dwarfs are only seen in the N band, and are exceptional objects. Consistent with what we found for the F band, three gm-type objects with unusually large N band κ-corrections correspond to three of the four galaxies noted in Paper I as having unusually red $N-K$ colors (sa68.10081, sa57.12508, and herc.3105). The fourth galaxy (sa68.5389) also has a N band κ-correction larger than any of the models. The final extreme outlier near $z=0.3$ (sa68.10356) is exceptional for having two image components with very different colors (one component was not even detected in the K band).

Which of our simple models is correct? If we believe the traditional models and observations, then the giant-dominated, two-star model seems more realistic. Independently, we know galaxies have an observed range of rest-frame $H-K$ colors of not much more than 0.2 mag for the majority of normal galaxies, for example as observed by Mobasher *et al.* (1986) in an optically selected sample of field galaxies. This implies that at $z=0.3$, where the observed K band is sampling the rest-frame H band wavelengths, the κ-corrections should have a spread of around 0.2 mag, and a smaller spread at lower redshifts. This line of reasoning would argue against the dwarf-dominated models. However a more definitive test can be made by inspecting the difference in dispersion of rest-frame color distribution predicted by the two sets of κ-corrections, which we discuss in the following section.

Since this is the first effort to produce observationally calibrated K band κ-corrections as a function of galaxy spectral type to significant redshift, we have made a more exhaustive comparison of the two-star model results (without K and M dwarfs) with what has been published previously.

The earliest published κ-corrections we have found are from Frogel *et al.* (1978b, see also Persson *et al.* 1979). Their κ-corrections are based on spectra of three late-type stars taken from stratoscope balloon observations of Woolf *et al.* (1964, spectral types K5III, M3III, and M2I). For the K band their κ-correction is a linear function of z with a slope

TABLE 2. Average K band κ-corrections.

z range	$\bar{z}$	$\bar{\kappa}$	$\sigma(\kappa)$	N
0.00−0.04	0.025	−0.08	0.02	11
0.04−0.08	0.070	−0.20	0.03	12
0.08−0.12	0.093	−0.25	0.03	30
0.12−0.16	0.135	−0.33	0.05	43
0.16−0.20	0.172	−0.42	0.04	18
0.20−0.24	0.228	−0.51	0.04	18
0.24−0.28	0.248	−0.55	0.04	11
0.28−0.32	0.303	−0.63	0.04	22

of −3.3 (note the sign change for consistency with our system). This agrees superbly with our results at low redshifts, namely $z<0.05$, which is well beyond the largest redshift in their survey. At higher redshifts, the same linear relation yields κ-corrections which are increasingly too negative compared to our results and the model curves in Fig. 9. This is not a serious concern because the Frogel *et al.*'s κ-correction formulas were presumably not meant to be extrapolated to such high redshift.

Near-infrared κ-corrections have been calculated explicitly at higher redshifts based on similar types of near-infrared stellar spectra. Although the κ-corrections from these spectra are unpublished, we include a description of some particularly sophisticated spectral compilations for completeness. For example, Puschell *et al.* (1982) used an evolving model from Bruzual (1981), in addition to their own nonevolving synthesis model. The latter consists of the Coleman *et al.* (1980) spectrum of the nuclear bulge of M31 for 0.14 to 1 μm, Whitford's (1971) measurements between 1.03 and 1.07 μm, and a synthesized spectrum using the population synthesis model of O'Connell (1976) with the spectrophotometry of Strecker *et al.* (1979), and Wolf *et al.* (1964). Likewise, a high resolution near-IR spectrum of the star α Tau has been

TABLE 3. (a) Absolute magnitudes and "free" two-star model parameters: bk and bg spectral-type galaxies.

NSER	Field	M_U	M_J	M_F	M_N	M_K	Star # hot	Star # cool	$f_{c,F}$
6589	sa68	-14.98 +0.03	-14.69 +0.03	-15.22 +0.03	-15.60 +0.07	-17.51 +0.17	75	135	0.64
14054	sa68	-16.15 +0.03	-15.99 +0.03	-16.52 +0.03	-17.05 +0.03	-18.49 +0.14	76	135	0.63
13429	sa57	-15.74 +0.03	-15.62 +0.03	-16.05 +0.03	-16.52 +0.10	-17.77 +0.10	77	131	0.56
13976	sa57	-17.36 +0.03	-17.19 +0.03	-17.70 +0.03	-18.25 +0.05	-19.80 +0.11	76	140	0.62
11920	sa68	-17.01 +0.03	-16.99 +0.03	-17.55 +0.03	-18.25 +0.03	-19.86 +0.12	77	141	0.65
2097	sa57	-17.55 +0.03	-17.46 +0.03	-18.04 +0.03	-18.55 +0.09	-20.26 +0.11	76	140	0.67
14358	herc1	-16.88 +0.04	-16.83 +0.03	-17.53 +0.03	-17.99 +0.14	-19.66 +0.12	74	135	0.76
2984	herc1	-18.30 +0.07	-17.92 +0.07	-18.35 +0.07	-18.87 +0.09	-20.28 +0.17	8	140	0.60
3848	herc1	-19.62 +0.04	-19.61 +0.04	-20.34 +0.04	-20.96 +0.04	-22.57 +0.08	76	140	0.74
17964	herc1	-19.50 +0.05	-19.96 +0.05	-21.05 +0.05	-21.76 +0.05	-23.51 +0.09	76	140	0.90
7917	sa68	-20.58 +0.02	-20.34 +0.03	-20.90 +0.03	-21.50 +0.03	-23.17 +0.08	75	140	0.68
14206	sa68	-19.24 +0.04	-19.12 +0.04	-19.84 +0.04	-20.51 +0.05	-22.20 +0.13	74	140	0.75
16752	herc1	-18.85 +0.10	-18.73 +0.09	-19.29 +0.11	-19.81 +0.21	-21.42 +0.14	76	140	0.67
13932	herc1	-19.11 +0.04	-19.03 +0.04	-19.70 +0.04	-20.39 +0.05	-21.81 +0.11	76	141	0.71
8663	herc1	-20.24 +0.03	-20.19 +0.02	-20.80 +0.03	-21.45 +0.08	-22.98 +0.07	77	141	0.65
13504[a]	sa68	-19.32 +0.03	-19.18 +0.02	-19.69 +0.04	-20.16 +0.11	-20.34 +1.18	10	53	0.73
16360	sa68	-19.58 +0.02	-19.49 +0.02	-20.12 +0.02	-20.78 +0.03	-22.38 +0.12	76	141	0.69
13330	sa57	-20.86 +0.02	-20.90 +0.02	-21.58 +0.02	-22.23 +0.03	-24.04 +0.10	11	140	0.71
17710	sa68	-20.20 +0.02	-20.30 +0.02	-21.18 +0.02	-21.91 +0.03	-23.77 +0.10	10	140	0.82
19264	sa57	-20.39 +0.06	-20.35 +0.07	-20.88 +0.08	-21.45 +0.10	-22.92 +0.06	12	140	0.63
12656	sa57	-20.38 +0.05	-20.28 +0.05	-20.74 +0.07	-21.26 +0.10	-22.72 +0.10	77	140	0.58
12909	sa57	-20.40 +0.02	-20.36 +0.02	-20.98 +0.04	-21.63 +0.07	-23.17 +0.08	11	141	0.66
3536	herc1	-19.70 +0.09	-19.81 +0.08	-20.46 +0.11	-20.99 +0.17	-22.58 +0.14	77	135	0.73
9673	herc1	-20.46 +0.09	-20.65 +0.08	-21.40 +0.11	-22.01 +0.15	-23.54 +0.16	13	135	0.76
5799	sa68	-20.53 +0.02	-20.54 +0.02	-21.20 +0.02	-21.84 +0.03	-23.51 +0.09	12	140	0.69
13536	sa68	-21.10 +0.02	-21.00 +0.02	-21.70 +0.02	-22.36 +0.03	-24.13 +0.09	10	140	0.73
9290	sa68	-21.11 +0.03	-21.04 +0.03	-21.68 +0.02	-22.30 +0.03	-23.96 +0.08	76	140	0.71
14712	sa68	-20.62 +0.03	-20.57 +0.03	-21.18 +0.04	-21.85 +0.05	-23.51 +0.10	11	141	0.65
11514	sa68	-20.65 +0.02	-20.56 +0.02	-21.23 +0.03	-21.89 +0.04	-23.45 +0.10	76	141	0.70
6689	sa57	-21.61 +0.03	-21.64 +0.02	-22.51 +0.05	-23.24 +0.05	-24.74 +0.04	12	141	0.76
13586	sa68	-20.98 +0.03	-21.02 +0.03	-21.86 +0.05	-22.59 +0.05	-24.25 +0.12	12	141	0.75
10585	sa68	-20.96 +0.03	-21.30 +0.03	-22.26 +0.05	-23.08 +0.05	-24.86 +0.13	12	141	0.84
12646	sa68	-19.07 +0.06	-19.23 +0.05	-19.96 +0.12	-20.66 +0.10	-22.35 +0.17	77	140	0.77
10334	sa68	-21.23 +0.03	-21.42 +0.03	-22.38 +0.04	-23.16 +0.08	-24.92 +0.30	13	141	0.79

Notes to TABLE 3(a)

[a] bg-type

TABLE 3. (b) Absolute magnitudes and "free" two-star model parameters: bm spectral-type galaxies.

NSER	Field	M_U	M_J	M_F	M_N	M_K	Star # hot	Star # cool	$f_{c,F}$
9494	sa57	-19.83 +0.03	-19.51 +0.08	-20.14 +0.12	-20.96 +0.09	-23.05 +0.02	74	153	0.64
7199	sa68	-18.65 +0.02	-18.51 +0.02	-19.10 +0.02	-19.83 +0.03	-21.55 +0.12	11	152	0.58
7723	sa68	-20.59 +0.02	-20.53 +0.03	-21.29 +0.03	-22.08 +0.05	-24.52 +0.10	13	153	0.65
7880	sa68	-20.23 +0.02	-20.25 +0.03	-21.09 +0.03	-21.95 +0.03	-24.02 +0.09	12	152	0.72
12423	herc1	-20.12 +0.03	-20.21 +0.04	-21.16 +0.04	-22.09 +0.03	-24.37 +0.08	13	153	0.76
5016	herc1	-20.13 +0.04	-20.20 +0.04	-21.06 +0.03	-22.00 +0.03	-24.15 +0.09	13	153	0.73
9695	sa68	-20.03 +0.02	-20.10 +0.02	-20.96 +0.02	-21.81 +0.03	-23.89 +0.07	13	152	0.73
16159	sa68	-18.98 +0.03	-19.06 +0.02	-19.93 +0.03	-20.80 +0.04	-22.64 +0.06	13	152	0.72
3174	herc1	-21.51 +0.02	-21.45 +0.02	-22.08 +0.02	-22.83 +0.03	-24.61 +0.07	13	152	0.60
3414	herc1	-21.20 +0.03	-21.55 +0.04	-22.65 +0.04	-23.62 +0.04	-25.72 +0.07	13	152	0.84
8506	sa57	-20.74 +0.02	-20.74 +0.02	-21.41 +0.02	-22.18 +0.03	-24.07 +0.07	13	152	0.64
3162	herc1	-20.68 +0.03	-20.85 +0.03	-21.80 +0.03	-22.72 +0.03	-24.67 +0.04	13	152	0.76
13576	sa68	-20.93 +0.02	-20.97 +0.02	-21.74 +0.02	-22.58 +0.03	-24.37 +0.07	13	152	0.69
9285	sa68	-21.01 +0.02	-21.09 +0.02	-22.00 +0.02	-22.91 +0.03	-24.78 +0.08	13	152	0.74
12006	sa68	-20.34 +0.02	-20.52 +0.02	-21.42 +0.02	-22.32 +0.03	-24.33 +0.06	13	152	0.76
6517	sa68	-21.68 +0.03	-21.78 +0.03	-22.63 +0.03	-23.50 +0.04	-25.45 +0.08	13	152	0.72
13222	herc1	-20.68 +0.03	-20.94 +0.02	-22.09 +0.04	-23.13 +0.05	-25.34 +0.06	13	153	0.83
12236	sa68	-20.89 +0.02	-20.88 +0.02	-21.56 +0.04	-22.35 +0.05	-24.15 +0.17	13	152	0.65
7928	herc1	-20.73 +0.03	-20.68 +0.02	-21.49 +0.02	-22.39 +0.05	-24.51 +0.30	12	153	0.70
11084	sa57	-22.62 +0.03	-22.77 +0.03	-23.57 +0.03	-24.47 +0.03	-26.57 +0.02	12	152	0.75
10356	sa68	-20.98 +0.03	-20.84 +0.04	-21.60 +0.08	-22.70 +0.09	-25.02 +0.32	13	156	0.61
15534	sa68	-20.43 +0.04	-20.55 +0.04	-21.27 +0.08	-22.15 +0.07	-24.16 +0.13	13	152	0.71
5154	sa68	-21.67 +0.03	-21.54 +0.03	-22.46 +0.05	-23.33 +0.05	-25.19 +0.14	13	153	0.70
10292	herc1	-25.06 +0.03	-24.54 +0.04	-24.63 +0.05	-25.08 +0.04	-26.76 +0.04	74	153	0.31

TABLE 3. (c) Absolute magnitudes and "free" two-star model parameters: am and ak spectral-type galaxies.

NSER	Field	M_U	M_J	M_F	M_N	M_K	Star # hot	Star # cool	$f_{c,F}$
10856	sa57	-18.32 +0.04	-18.28 +0.09	-18.44 +0.04	-18.76 +0.05	-20.49 +0.07	19	164	0.04
13616	herc1	-19.46 +0.04	-20.15 +0.04	-21.36 +0.04	-22.33 +0.06	-24.47 +0.03	24	153	0.80
11651	sa68	-19.59 +0.03	-20.25 +0.03	-21.36 +0.04	-22.34 +0.05	-24.33 +0.07	83	152	0.77
11859	herc1	-21.14 +0.03	-21.45 +0.03	-22.45 +0.03	-23.40 +0.03	-25.44 +0.03	15	153	0.73
15295	sa68	-19.66 +0.03	-20.02 +0.02	-21.07 +0.02	-22.01 +0.03	-23.98 +0.05	80	152	0.78
10153	sa68	-20.27 +0.02	-20.66 +0.02	-21.70 +0.02	-22.68 +0.03	-24.87 +0.04	79	153	0.78
18231	sa57	-20.78 +0.02	-21.06 +0.02	-21.82 +0.03	-22.61 +0.05	-24.50 +0.05	17	152	0.63
16664	sa68	-20.41 +0.02	-20.72 +0.02	-21.71 +0.02	-22.66 +0.03	-24.80 +0.06	80	153	0.75
16380	sa68	-21.08 +0.02	-21.37 +0.02	-22.23 +0.02	-23.13 +0.03	-25.13 +0.06	79	152	0.72
7001	sa68	-20.64 +0.02	-21.12 +0.02	-22.11 +0.02	-23.03 +0.03	-25.13 +0.06	17	152	0.77
11746	sa68	-20.39 +0.03	-21.00 +0.02	-22.07 +0.02	-23.02 +0.03	-25.09 +0.05	81	152	0.77
6356	sa68	-20.97 +0.02	-21.32 +0.02	-22.22 +0.02	-23.11 +0.04	-25.27 +0.23	79	152	0.74
17481	sa57	-21.83 +0.08	-22.25 +0.08	-23.09 +0.09	-23.93 +0.10	-25.90 +0.03	81	152	0.64
10554	herc1	-22.25 +0.03	-22.55 +0.03	-23.40 +0.03	-24.25 +0.03	-26.17 +0.04	17	152	0.66
17778	herc1	-21.42 +0.03	-21.64 +0.03	-22.53 +0.05	-23.42 +0.06	-25.41 +0.06	79	153	0.68
3176	herc1	-21.19 +0.04	-21.74 +0.03	-22.86 +0.05	-23.82 +0.05	-25.90 +0.06	83	153	0.73
12301	sa57	-21.10 +0.03	-21.33 +0.03	-22.22 +0.07	-23.01 +0.07	-24.69 +0.04	17	152	0.59
11790	sa68	-21.86 +0.03	-22.29 +0.04	-23.30 +0.04	-24.19 +0.04	-26.09 +0.04	18	152	0.72
8317[a]	herc1	-20.83 +0.03	-21.38 +0.03	-22.39 +0.03	-23.15 +0.03	-24.74 +0.06	79	141	0.83
10973	herc1	-22.09 +0.03	-22.49 +0.03	-23.68 +0.05	-24.64 +0.04	-26.66 +0.04	14	153	0.78
3756	herc1	-22.22 +0.03	-22.65 +0.03	-23.72 +0.03	-24.64 +0.03	-26.62 +0.04	20	152	0.75
14271	sa68	-20.19 +0.06	-20.33 +0.06	-21.37 +0.09	-22.15 +0.08	-23.85 +0.07	80	152	0.64
7997	sa68	-22.02 +0.03	-22.25 +0.03	-23.23 +0.03	-24.13 +0.03	-26.09 +0.14	79	153	0.73
6024	sa68	-22.10 +0.03	-22.28 +0.03	-23.19 +0.03	-24.09 +0.14	-26.14 +0.64	79	153	0.70
5617[a]	sa68	-21.15 +0.03	-21.77 +0.03	-22.79 +0.03	-23.57 +0.03	-25.28 +0.08	83	141	0.78
12670	sa68	-20.01 +0.05	-19.96 +0.05	-20.79 +0.10	-21.47 +0.09	-23.25 +0.11	80	153	0.50
1279	sa68	-22.25 +0.03	-22.60 +0.03	-23.57 +0.03	-24.50 +0.04	-26.51 +0.18	14	153	0.74

Notes to TABLE 3(c)

[a] ak-type

TABLE 3. (d) Absolute magnitudes and "free" two-star model parameters: fm spectral-type galaxies.

NSER	Field	M_U	M_J	M_F	M_N	M_K	Star # hot	Star # cool	$f_{c,F}$
1564	sa57	-16.91 +0.04	-17.12 +0.03	-17.90 +0.03	-18.65 +0.07	-20.27 +0.09	33	153	0.35
17315	sa68	-17.26 +0.03	-17.43 +0.03	-18.28 +0.03	-19.05 +0.03	-20.81 +0.07	32	153	0.41
8676	sa57	-19.07 +0.04	-19.21 +0.04	-19.76 +0.04	-20.25 +0.09	-22.08 +0.09	91	164	0.04
5009	hercl	-19.59 +0.03	-19.82 +0.03	-20.69 +0.03	-21.64 +0.03	-23.65 +0.03	36	156	0.34
6095	hercl	-19.33 +0.03	-19.59 +0.03	-20.57 +0.03	-21.40 +0.04	-23.20 +0.07	36	153	0.43
5389	sa68	-20.55 +0.02	-20.63 +0.02	-21.32 +0.03	-22.20 +0.03	-24.72 +0.12	35	165	0.09
3161	hercl	-19.76 +0.03	-19.90 +0.03	-20.79 +0.03	-21.61 +0.03	-23.61 +0.06	36	156	0.29
17050	hercl	-19.77 +0.03	-20.18 +0.03	-21.27 +0.04	-22.14 +0.05	-24.27 +0.08	153	32	0.37
15439	hercl	-19.68 +0.03	-20.37 +0.03	-21.59 +0.04	-22.46 +0.05	-24.63 +0.08	152	91	0.26
6062	sa57	-19.91 +0.06	-20.10 +0.08	-20.98 +0.08	-21.80 +0.10	-23.59 +0.04	34	153	0.42
13618	hercl	-18.93 +0.02	-19.08 +0.02	-19.88 +0.02	-20.61 +0.03	-22.40 +0.04	36	156	0.22
13612	hercl	-19.08 +0.02	-19.43 +0.02	-20.45 +0.02	-21.49 +0.03	-23.74 +0.04	36	156	0.48
13213	sa68	-19.09 +0.02	-19.38 +0.02	-20.33 +0.02	-21.27 +0.03	-23.41 +0.06	36	156	0.41
11277	sa68	-19.32 +0.02	-19.48 +0.02	-20.31 +0.02	-21.15 +0.03	-23.08 +0.08	35	156	0.27
12487	sa68	-20.85 +0.03	-21.31 +0.04	-22.44 +0.06	-23.57 +0.11	-25.79 +0.09	156	36	0.43
16662	hercl	-19.44 +0.03	-19.71 +0.03	-20.70 +0.03	-21.53 +0.03	-23.46 +0.05	153	34	0.50
6357	hercl	-20.47 +0.03	-21.14 +0.04	-22.29 +0.04	-23.21 +0.06	-25.25 +0.08	152	87	0.25
14871	sa57	-20.73 +0.06	-20.96 +0.08	-21.84 +0.08	-22.60 +0.11	-24.44 +0.02	32	153	0.44
8069	hercl	-20.29 +0.03	-20.62 +0.03	-21.66 +0.04	-22.51 +0.04	-24.36 +0.03	36	153	0.49
7872	sa57	-21.56 +0.07	-21.84 +0.08	-22.43 +0.08	-23.01 +0.11	-24.61 +0.06	31	152	0.30
12163	hercl	-20.34 +0.02	-20.72 +0.03	-21.73 +0.03	-22.54 +0.03	-24.49 +0.04	153	34	0.47
8541	hercl	-20.72 +0.03	-20.90 +0.03	-21.73 +0.02	-22.56 +0.03	-24.40 +0.06	35	156	0.26
10720	hercl	-20.69 +0.04	-21.32 +0.03	-22.47 +0.03	-23.43 +0.04	-25.49 +0.05	153	86	0.27
10463	hercl	-21.72 +0.04	-22.04 +0.04	-22.94 +0.04	-23.90 +0.04	-26.12 +0.07	34	156	0.44
16944	sa57	-21.59 +0.07	-21.89 +0.07	-22.75 +0.08	-23.50 +0.10	-25.31 +0.04	32	152	0.47
17604	sa57	-21.44 +0.02	-21.65 +0.02	-22.49 +0.03	-23.31 +0.04	-25.14 +0.06	36	156	0.27
1906	hercl	-21.09 +0.04	-21.49 +0.02	-22.64 +0.04	-23.57 +0.04	-25.50 +0.03	153	34	0.38
1693	sa68	-21.25 +0.02	-21.67 +0.02	-22.70 +0.03	-23.57 +0.03	-25.46 +0.04	152	33	0.41
9243	sa57	-21.36 +0.03	-21.84 +0.02	-22.82 +0.05	-23.66 +0.05	-25.59 +0.03	152	91	0.42
12290	sa68	-21.47 +0.03	-21.77 +0.03	-22.71 +0.03	-23.56 +0.14	-25.67 +0.64	153	32	0.49
16599	sa57	-21.49 +0.03	-21.90 +0.03	-22.70 +0.05	-23.45 +0.05	-25.27 +0.03	152	87	0.49
12666	sa68	-21.17 +0.03	-21.76 +0.03	-22.89 +0.03	-23.74 +0.04	-25.46 +0.17	152	40	0.40
6217	sa68	-20.97 +0.03	-21.53 +0.03	-22.56 +0.04	-23.44 +0.03	-25.37 +0.08	152	88	0.34
6699	sa68	-20.69 +0.04	-21.21 +0.03	-22.25 +0.05	-23.16 +0.04	-25.20 +0.07	153	31	0.36
5841	sa68	-21.33 +0.03	-21.85 +0.03	-22.89 +0.03	-23.79 +0.04	-25.83 +0.18	153	88	0.36
17144	sa68	-21.69 +0.04	-22.35 +0.04	-23.50 +0.04	-24.39 +0.04	-26.24 +0.08	152	40	0.37

TABLE 3. (e) Absolute magnitudes and "free" two-star model parameters: gm spectral-type galaxies.

NSER	Field	M_U	M_J	M_F	M_N	M_K	Star # hot	Star # cool	$f_{c,F}$
16453	sa57	-18.28 +0.07	-18.90 +0.10	-19.78 +0.09	-20.33 +0.11	-22.04 +0.03	52	165	0.03
4072	sa57	-17.74 +0.07	-18.14 +0.09	-19.19 +0.09	-19.90 +0.11	-21.73 +0.05	93	153	0.43
1289	sa57	-19.34 +0.07	-19.95 +0.09	-20.97 +0.09	-21.84 +0.11	-23.73 +0.02	98	156	0.25
7975	herc1	-19.05 +0.05	-19.68 +0.03	-20.65 +0.03	-21.51 +0.05	-23.44 +0.04	52	162	0.11
17344	herc1	-18.93 +0.05	-19.51 +0.03	-20.68 +0.03	-21.75 +0.05	-23.95 +0.03	47	156	0.50
3869	sa57	-20.88 +0.07	-21.42 +0.09	-22.52 +0.09	-23.32 +0.11	-25.24 +0.02	152	93	0.44
10081	sa68	-20.79 +0.02	-20.99 +0.02	-21.85 +0.03	-22.99 +0.03	-25.54 +0.10	93	164	0.19
3861	sa57	-20.68 +0.06	-21.35 +0.08	-22.35 +0.08	-23.09 +0.11	-24.96 +0.02	52	156	0.20
12508	sa57	-18.71 +0.09	-19.35 +0.02	-20.41 +0.04	-21.60 +0.08	-24.01 +0.05	52	162	0.27
16215	herc1	-19.89 +0.04	-20.72 +0.05	-21.94 +0.05	-22.82 +0.06	-24.79 +0.13	153	98	0.48
14852	sa57	-19.21 +0.07	-19.83 +0.02	-20.74 +0.04	-21.54 +0.09	-23.46 +0.07	52	163	0.09
11544	sa57	-19.83 +0.05	-20.52 +0.03	-21.49 +0.03	-22.33 +0.05	-24.30 +0.04	103	165	0.06
10962	sa57	-19.65 +0.05	-20.29 +0.02	-21.27 +0.03	-22.12 +0.04	-24.21 +0.05	54	164	0.07
16036	sa57	-19.88 +0.04	-20.56 +0.03	-21.55 +0.03	-22.47 +0.05	-24.39 +0.06	103	162	0.11
13044	sa57	-20.42 +0.02	-20.86 +0.02	-21.88 +0.02	-22.86 +0.03	-24.98 +0.05	45	156	0.41
12493	sa57	-19.36 +0.05	-20.11 +0.02	-21.13 +0.03	-21.97 +0.04	-23.86 +0.05	52	156	0.24
17300	sa57	-20.12 +0.06	-20.74 +0.07	-21.75 +0.08	-22.59 +0.10	-24.62 +0.04	50	156	0.30
6578	sa57	-20.79 +0.03	-21.13 +0.02	-22.03 +0.03	-22.80 +0.05	-24.46 +0.07	41	153	0.35
13343	sa57	-20.60 +0.03	-21.26 +0.03	-22.26 +0.05	-23.16 +0.09	-25.02 +0.06	54	162	0.09
12019	sa57	-20.11 +0.03	-20.75 +0.03	-21.89 +0.03	-22.68 +0.05	-24.70 +0.06	153	47	0.47
6463	sa57	-21.13 +0.06	-21.88 +0.08	-23.03 +0.09	-23.81 +0.12	-25.82 +0.02	153	95	0.47
14166	sa57	-20.79 +0.07	-21.41 +0.08	-22.39 +0.09	-23.29 +0.13	-25.18 +0.03	52	162	0.11
11014	sa57	-21.58 +0.03	-22.38 +0.04	-23.59 +0.06	-24.68 +0.10	-26.53 +0.03	54	156	0.33
4389	herc1	-18.79 +0.09	-19.35 +0.02	-20.42 +0.05	-21.24 +0.09	-23.05 +0.10	47	152	0.47
4309	herc1	-19.46 +0.08	-19.83 +0.05	-20.72 +0.07	-21.60 +0.11	-23.63 +0.09	45	156	0.31
14054	sa57	-19.92 +0.05	-20.59 +0.02	-21.59 +0.03	-22.52 +0.04	-24.54 +0.03	54	162	0.13
10005	sa57	-20.64 +0.03	-21.24 +0.03	-22.18 +0.02	-23.04 +0.03	-24.95 +0.07	52	162	0.10
14293	sa57	-20.66 +0.06	-21.35 +0.07	-22.47 +0.08	-23.28 +0.12	-25.23 +0.03	153	95	0.50
15041	sa57	-19.82 +0.05	-20.56 +0.02	-21.58 +0.03	-22.40 +0.04	-24.32 +0.04	52	156	0.24
3105	herc1	-20.31 +0.05	-20.97 +0.02	-22.16 +0.03	-23.29 +0.04	-25.59 +0.04	156	47	0.43
10849	herc1	-20.36 +0.03	-20.96 +0.03	-22.16 +0.03	-23.11 +0.03	-24.98 +0.04	152	41	0.36
3873	sa68	-19.79 +0.04	-20.41 +0.02	-21.37 +0.02	-22.22 +0.03	-24.14 +0.06	98	156	0.24
13756	sa57	-20.97 +0.04	-21.62 +0.02	-22.66 +0.02	-23.66 +0.03	-25.61 +0.05	100	163	0.13
10882	sa57	-21.48 +0.03	-22.35 +0.03	-23.40 +0.06	-24.26 +0.08	-26.29 +0.06	110	164	0.06
7693	sa57	-19.60 +0.09	-20.24 +0.02	-21.63 +0.09	-22.57 +0.09	-24.35 +0.04	153	41	0.38
10468	sa57	-20.90 +0.05	-21.52 +0.03	-22.53 +0.05	-23.46 +0.06	-25.58 +0.03	54	164	0.08
10506	sa57	-20.12 +0.06	-20.89 +0.02	-22.00 +0.07	-22.93 +0.07	-24.92 +0.03	100	156	0.30
12482	sa57	-19.67 +0.11	-20.38 +0.05	-21.41 +0.14	-22.38 +0.14	-24.53 +0.10	52	156	0.35
9542	sa57	-20.40 +0.05	-20.97 +0.02	-22.09 +0.07	-22.97 +0.07	-24.91 +0.04	153	45	0.46
6840	herc1	-21.22 +0.04	-21.77 +0.03	-22.98 +0.05	-23.88 +0.05	-25.77 +0.04	153	45	0.45
10630	sa57	-20.94 +0.04	-21.62 +0.03	-22.64 +0.05	-23.64 +0.05	-25.63 +0.05	103	162	0.13
12260	sa57	-21.03 +0.04	-21.79 +0.03	-22.88 +0.04	-23.85 +0.04	-25.90 +0.05	52	156	0.34
12053	sa57	-22.42 +0.03	-22.82 +0.02	-24.16 +0.03	-25.08 +0.03	-26.99 +0.03	153	93	0.40
11827	sa57	-21.02 +0.04	-21.74 +0.03	-22.81 +0.05	-23.74 +0.04	-25.75 +0.05	52	156	0.30
13900	sa57	-21.16 +0.03	-21.82 +0.03	-22.84 +0.04	-23.80 +0.04	-25.79 +0.05	100	162	0.13
5165	sa57	-21.66 +0.03	-22.32 +0.03	-23.48 +0.03	-24.34 +0.03	-26.12 +0.05	49	153	0.46
18052	herc1	-21.54 +0.03	-22.18 +0.03	-23.41 +0.07	-24.35 +0.06	-26.34 +0.04	153	45	0.38
7660	sa68	-20.52 +0.05	-21.11 +0.03	-22.36 +0.04	-23.24 +0.04	-25.02 +0.08	152	93	0.39
11061	sa68	-19.78 +0.09	-20.39 +0.05	-21.37 +0.09	-22.20 +0.08	-24.05 +0.08	98	156	0.23
13903	sa68	-19.95 +0.09	-20.58 +0.05	-21.65 +0.08	-22.43 +0.07	-24.16 +0.13	50	153	0.35
5110	herc1	-22.15 +0.03	-22.70 +0.03	-24.07 +0.05	-25.00 +0.04	-26.96 +0.05	153	93	0.35
3811	herc1	-21.32 +0.08	-22.02 +0.06	-23.16 +0.06	-24.02 +0.06	-25.85 +0.09	49	153	0.46

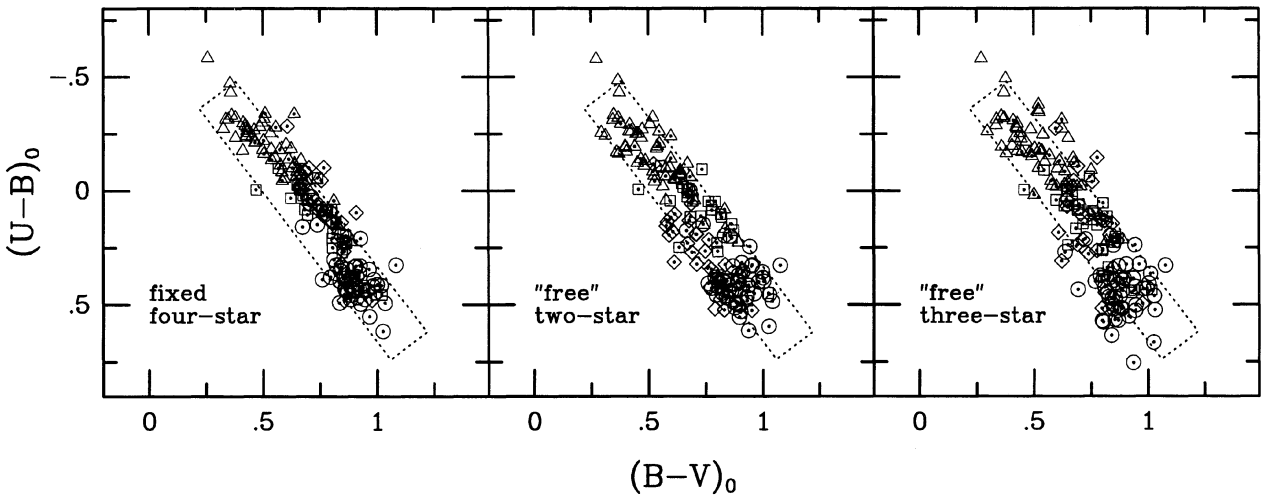

FIG. 10. The rest-frame $U-B, B-V$ two-color distribution as derived from the fixed four-star model (left panel), "free" two-star model (middle panel), and "free" three-star model (right panel) for all galaxies in our sample except those with >20% saturation in any band. Objects are marked as in Fig. 8. The dotted rectangle is adopted from Huchra (1977), as described in the text to enclose 92% of all local galaxies from his field sample.

used in several studies to model κ-corrections for early-type galaxies (Lebofsky 1981; Lilly 1983). Lebofsky, in her study of high redshift giant elliptical galaxies, modified this spectrum to have the same CO and H_2O indices found for giant ellipticals, and used existing spectra of ellipticals at optical wavelengths.

Mobasher *et al.* (1986) present the only published data for near-IR κ-corrections for field galaxies. As shown in Fig. 9, their K band κ-corrections, which are applicable for $z \leq 0.1$, appear to be small relative to our measurements. Because of this discrepancy, we have examined and summarize here their method to derive κ-corrections, which is based on polynomial fits to the observed broadband color-redshift distributions. First they corrected all E/S0 galaxies' colors in their sample to those for a single luminosity, based on E/S0 color–luminosity relations established locally by other work. Then they fit a polynomial to $B-K$ vs z, and adopted B band κ-corrections from Pence on the basis of morphological type to derive the K band κ-corrections. They have built into their estimation of the κ-corrections the assumption that in the near-IR the κ-corrections are the same for all galaxies. This assumption appears to be reasonably accurate in the K band at low z. However, it is puzzling that they present only a single equation for the $B-K$ κ-correction since galaxies have a wide range in $B-K$ color and hence κ-correction. Although we have been unable to ascertain why Mobasher *et al.*'s K band κ-corrections are different than ours, their's are also inconsistent with the models of BC93 and spectral observations of local galaxies.

Finally, Eisenhardt & Lebofsky (1987) have published a polynomial expression for the κ-correction in the H and K bands, which is constructed from UV data from Bruzual (1981), optical data to 1 μm from Whitford (1971) and Gunn *et al.* (1981), and Fourier transform spectroscopy of M32 and the nucleus of M31 from 1–2.45 μm (Lebofsky & Rieke 1987). Note that Eisenhardt and Lebofsky's H band is somewhat unconventional, but they give adequate information to transform their bands into a standard system. Their K band κ-correction is somewhat larger (less negative) than models and other observations, but it provides a nice envelope for the κ-corrections derived from our two-star model.

We have tabulated the mean κ-corrections for the K band in intervals of 0.04 in redshift for our sample (Table 2). The dispersion in each redshift interval (as well as the mean redshift in the interval) are also included. The dispersion includes the trend of the κ-correction within each finite redshift bin, and so is an upper limit on the intrinsic dispersion at a given redshift. The K band κ-correction, because of its small dispersion and particular correlation with redshift, can be approximated well for all galaxies by a single power-law in the the range $0<z<0.3$. A power-law index α between 0.67–1.67 provides an upper and lower envelope which spans the observed κ-corrections in this redshift range. A good intermediate value of α is 1.25. For the majority of galaxies in our sample, K band κ-corrections estimated with such a power-law agree to better than 5% with the values calculated by method (4).

4. REST-FRAME COLORS

Absolute magnitudes in all bands for spectrally classified galaxies in our sample are presented here in Tables 3(a)–

[6]This error estimate does not include systematic or additional random errors introduced by the interpolation process, since we have not determined their magnitude. Such an estimate could be made either via some Monte Carlo procedure, or simulations. We expect the magnitude of the errors introduced via the interpolation process to be small because the models are reasonably accurate (i.e., physical) representations of the true SEDs, and they fit the observed broadband data well. We have neglected these errors here because our results do not depend on more precise values for the *rest-frame* photometric errors.

3(e), matching Tables 6(a)–6(e) from Paper I. Rest-frame colors can be derived from these data. The last three columns of the tables contain the stellar fraction ($f_{c,F}$) from the "free" two-star model described in Sec. 2, as well as the two "ID" numbers of the hot and cool stars, referenced to Gunn & Stryker (1983).

Absolute magnitudes were derived using the κ-corrections described in the previous section, and assuming a standard cosmology with the Hubble constant $H_0=50$, the deacceleration parameter $q_0=0.1$, and the cosmological constant $\Lambda_0=0$. All absolute magnitudes are scaled to the K total apparent magnitudes from Paper I. As in Tables 6(a)–6(e) (Paper I) photometric errors are quoted in Tables 3(a)–3(e) for the positive root of the error function. However, recall that to derive an effective κ-correction for each band we have interpolated via the models between the two observed bands that bracket the redshifted band of interest. Effectively, then, we form a weighted average of two observed bands, and we derive the photometric errors for each rest-frame magnitude accordingly, including as well the error introduced by scaling matched-aperture magnitudes to total magnitudes.[6] Note that the photometric errors for colors formed from data in Tables 3(a)–3(e) are not necessarily the quadrature sum of magnitude errors (i.e., the formula given in the notes to Table 6 of Paper I) because the rest-frame magnitude errors may be correlated via the bracketing procedure. In the following analysis we have derived the correct color errors when necessary. Also note that Tables 3(a)–3(e) still contain galaxies with saturated photometry, etc., and the reader should refer back to Tables 6(a)–6(e) of Paper I for these flags.

A final test and the culmination of our photometric modeling efforts is to compare the rest-frame color distribution of our galaxies with local samples. Because there is little photometry of local galaxies in our photographic bands, we first take advantage of our models and method for calculating κ-corrections to derive multicolor distributions in standard, photoelectric systems. This can be done in a straightforward and reliable way with knowledge of the filter response curves, as described in Sec. 3. Given the relative availability of photometry in particular bands for large samples of local galaxies, as well as the desire to explore the blue and red extremes of our sampled wavelength range, we have chosen first to simulate UBV and $J_{\rm IR}HK$ colors. We then explore the distribution of spectral types in the UVK plane.

4.1 The UBV Plane

The rest-frame UBV multicolor distribution for all galaxies in our sample (except for galaxies with >20% saturation in any band) is shown in Fig. 10. The colors derived from each of the three simple models we have considered, namely 4 fixed stars, and "free" 2 and 3 stars, have been plotted separately. To facilitate a comparison with Huchra (1977), we have adopted the filter transmission curves of Matthews & Sandage (1963), which should best represent his photometric system. A rectangle has been drawn in each panel of Fig. 10, as defined by Huchra (1977) to enclose 92% of the 366 fields galaxies in his sample. A comparison of his Fig. 2(a) with Fig. 10 shows a remarkable agreement. This attests

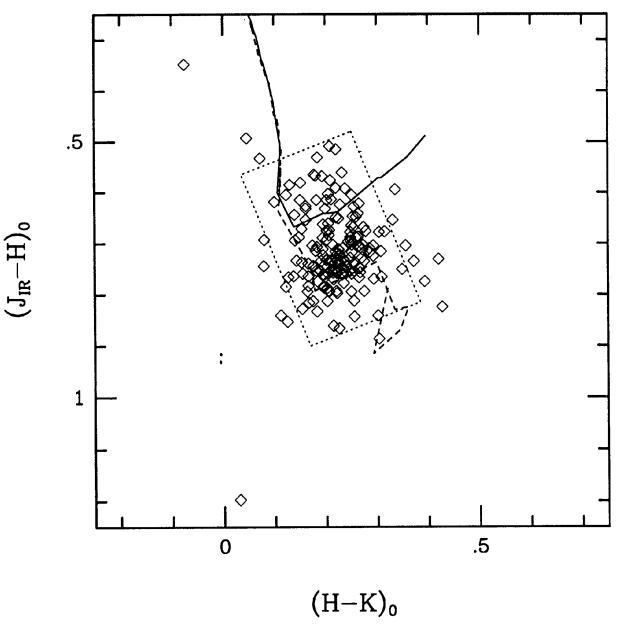

FIG. 11. The rest-frame $J_{\rm IR}-H$, $H-K$ two-color distribution for galaxies from Mobasher *et al.* (1986). For comparison, the loci of main-sequence and giant stars from the spectral library of BC93 are shown as solid and dashed lines, respectively. The dotted rectangle, described in the text, is defined on the basis of this figure to be roughly analogous to the rectangle in Fig. 10.

to the absolute calibration of both our photometry, models, and derived κ-corrections (which in this case include a photometric transformation).

We have plotted the results of the three simple models to reinforce our earlier conclusions concerning the relative abilities of these models to reproduce the range of observed galaxy colors. The fixed, four-star model locus is much tighter than for either of the "free" models, as well as the distribution shown by Huchra. This is presumably an artifact of the model not having enough freedom to accurately represent the full range of observed colors. It is difficult to decide whether one of the two- or three-star model is significantly better than the other. On the one hand the three-star model does show the slight curvature with respect to the rectangle seen in Fig. 2(a) of Huchra, whereas the scatter of the two-star model seems more comparable to this same figure. As we indicated earlier, we have chosen the two-star model for reasons of simplicity.

4.2 The $J_{IR}HK$ Plane

One of the most exacting comparisons to make is whether we can reproduce the rest-frame near-infrared $J_{\rm IR}-H$, $H-K$ multicolor distribution of galaxies. This is particularly challenging because of the large gap (roughly 1 μm) in sampled wavelength between the N and K bands. This comparison, for which we will refer to the large sample of fields galaxies from Mobasher *et al.* (1986), will provide a test of how well the simple models reproduce the spectral region dominated by cool stars.

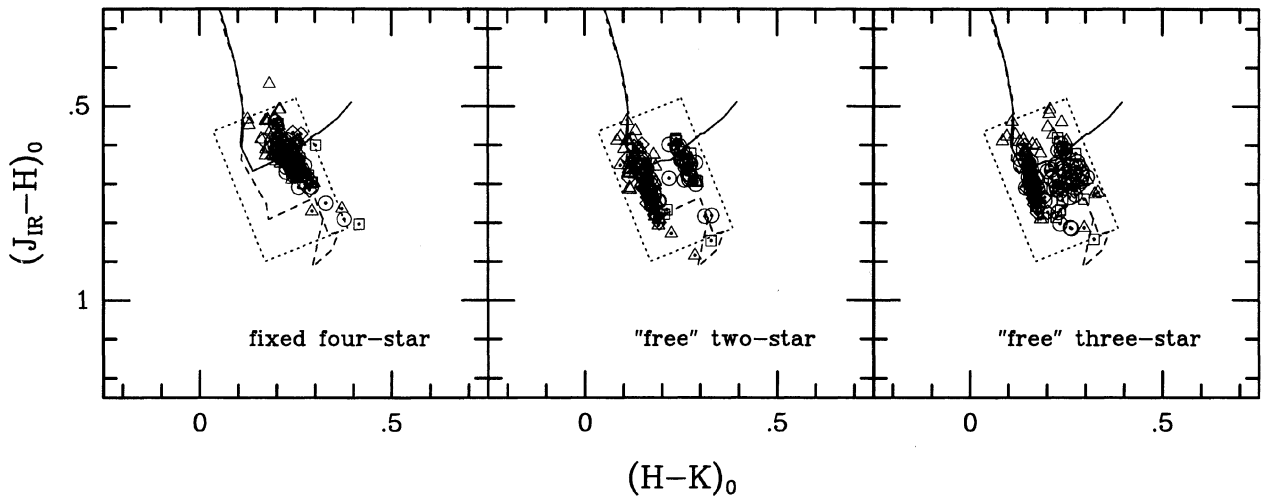

FIG. 12. The rest-frame $J_{IR}-H$, $H-K$ two-color distribution as derived from the fixed four-star model (left panel), "free" two-star model (middle panel), and "free" three-star model (right panel) for all galaxies in our sample except those with >20% saturation in any band. Objects are marked as in Fig. 8. The loci of main sequence and giant stars from the spectral library of BC93 are shown as solid and dashed lines, respectively. The dotted rectangle is the same as in Fig. 11.

To correct the Mobasher *et al.* colors to the rest-frame we have adopted their κ-corrections for the $J_{IR}-H$ and $H-K$ colors. Although we found that their polynomial expression for the K band κ-correction did not agree with other results, their polynomial expression for the $H-K$ κ-correction does agree with both Frogel *et al.* (1978b) for $z<0.05$ and with BC93 models for $z<0.1$, which is the redshift limit of their survey. Their $J_{IR}-H$ κ-correction differs in sign and absolute amplitude from that of Frogel *et al.*, but agrees with the BC93 models. The resulting rest-frame multicolor distribution is shown in Fig. 11. The colors are consistent with samples of more local galaxies (e.g., Aaronson 1977; Griersmith *et al.* 1982; Glass 1984).

For reference we have plotted the stellar loci of the main-sequence and giant stars from the BC93 library. These colors were calculated using filter response curves appropriate for the California Institute of Technology (CIT) near-infrared photometric system (Elias *et al.* 1982). Although Mobasher *et al.* set their photometric zero-points from observations of standard stars from Elias *et al.* (1982), which defines the CIT system, they subsequently converted their photometry to the "Johnson"[7] system on the basis of transformations in Frogel *et al.* (1978b). On the basis of the extensive compilations and comparisons of different near-infrared photometric systems by Bessell & Brett (1988), we estimate that differences between these two systems ("Johnson" and CIT) amount to 0.06 mag in $J_{IR}-H$ and 0.03 mag for $H-K$ for the average colors of the galaxies in the Mobasher *et al.* sample, in the sense that the CIT colors are bluer. Even taking this into account, most of the galaxies lie to the red in $J_{IR}-H$ and $H-K$ of the main sequence, as shown for E and S0 galaxies by Frogel *et al.* (1978b), and for S0 to Sd galaxies by Aaronson (1977). This is further evidence that giant stars must dominate the light in the near infrared.

We have defined a rectangle around the Mobasher *et al.* galaxy distribution, in analogy to what Huchra did for galaxies in the *UBV* plane. The rectangle center has colors of $J_{IR}-H=0.72$ and $H-K=0.22$, a width of 0.23 mag and a height of 0.36 mag, and is aligned to be roughly parallel with the stellar locus prior to the bifurcation of dwarf and giant stars. This same rectangle is then super-imposed on Fig. 12, which contains the simulated rest-frame $J_{IR}HK$ plane for our galaxies, again on the basis of the three simple models. What is immediately evident from this figure is that the model using four fixed stellar types is clearly inadequate at reproducing the mean or full range of $J_{IR}-H$ and $H-K$ colors found in the Mobasher *et al.* sample. One may infer that at least one more stellar type would have to be added to fit all bands ($UJFNJ_{IR}HK$). The "free" three-star model has a range and distribution in color most comparable to the observed distribution in Fig. 11. However, the "free" two-star model has the same range in color, and merely shows a bimodal distribution with a gap of about 0.1 mag. Galaxies in the redder clump (in $H-K$) are modeled with cool stars from the library corresponding to No. 156 or larger (see Fig. 7). These stars are 0.1 mag redder in $H-K$ than earlier stars, and hence this bimodality is not a limit of the two-star model as a class, but a reflection of the library. (This change in stellar color can be seen in Fig. 12 as the sudden, right-angled shift to redder $H-K$ in the giant locus occurring at a $J_{IR}-H=0.8$.)

Note that in terms of the κ-corrections for the K band derived in the previous section for the "free" two-star model, there is at *most* an 0.05 mag systematic error due to this artificial bifurcation seen in Fig. 12. The sign of the error is correlated with the intrinsic near-infrared color. However, the average colors are in excellent agreement with the Mobasher

[7]Reference to the Johnson photometric system as defined by Johnson (1966) is not strictly correct since in this paper Johnson did not define an H band.

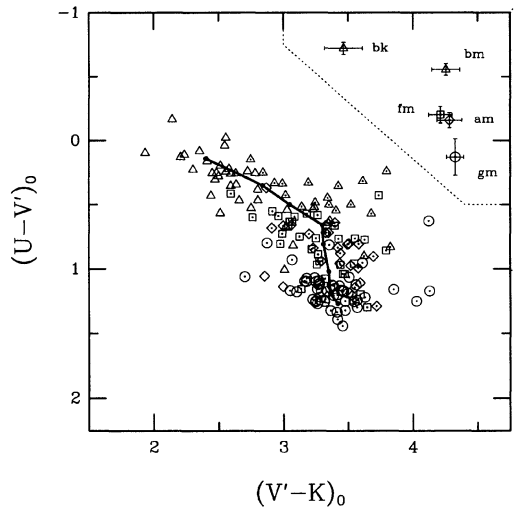

FIG. 13. The rest-frame $U-V'$, $V'-K$ two-color distribution of our galaxy sample, as derived from the "free" two-star model, where $V'\equiv(J+F)/2$. Objects are marked as in Fig. 8. Galaxies with >20% saturation in any band have been excluded. The locus of colors as a function of Hubble type from Aaronson (1978) is shown as a solid line. The transformation between his photometric system to ours is described in the text. The characteristic photometric errors for each galaxy spectral type are represented in the upper-right corner of the diagram. These error bars are placed in the same relative positions as the mean colors for each spectral type.

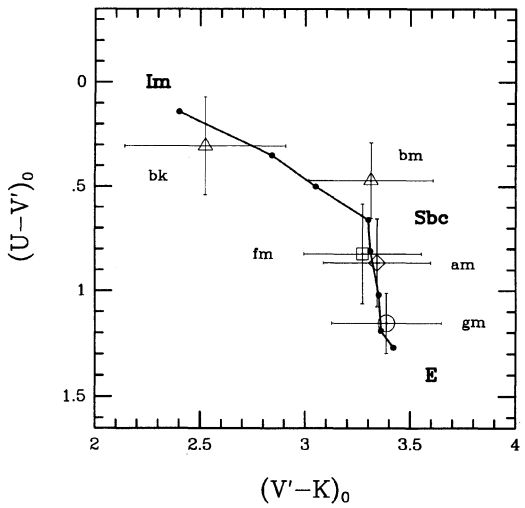

FIG. 14. The distribution of mean colors for rest-frame $U-V'$ and $V'-K$ for different spectral types and Hubble types. Error bars represent the standard deviation of colors within each spectral type. Mean colors for Hubble types are derived as discussed in the text. Mean colors for spectral types are listed in Table 4.

et al. distribution. Similarly, on average the K band κ-corrections, as tabulated in Table 2, should be unaffected by this bimodality. It is remarkable that such a simple model can reproduce the mean and range of colors in a region of the spectrum between 0.9 and 1.9 μm which was not even measured.

4.3 The UVK Plane

Perhaps the best way to visually compare the rest-frame color distribution of our galaxies with local samples is in the UVK plane. This is because the distribution of galaxies in this color space has been well studied both observationally and theoretically, and it represents the broadest color baseline that we can construct from our data. To do this, we plot photographic $U-(J+F)/2$ vs $(J+F)/2$-K. The composite magnitude $(J+F)/2$, which we will define as V', is similar to the standard V band, although much broader. The comparison of these data to the mean $U-V$ and $V-K$ color distribution of Aaronson's (1978) sample is ideal because he has photometered galaxies across the spectrum of Hubble types. We use the transformation of Kron (1980) between J,F and B,V, and Huchra's (1977) $U-B$ and $B-V$ colors for a sample comparable to Aaronson's to transform Aaronson's $U-V$ and $V-K$ to our system. There is excellent agreement between our rest-frame colors and Aaronson's, as displayed in Fig. 13.

Had we used the κ-corrections from the dwarf-dominated two-star model, the reddest galaxies in $V'-K$ would be stretched by up to about 0.2 mag farther to the red in $V'-K$. The tightness of the locus in Fig. 13 using the giant-dominated models is further, and final evidence that the models are reasonably correct. In fact, the dispersion of our locus for redder galaxies is quite comparable to the dispersion in Fig. 1 of Aaronson (1978). For bluer galaxies, our significantly larger sample makes such a comparison difficult.

To avoid spurious, outlying objects in Fig. 13 we have eliminated galaxies with severely saturated photometry, as before. We have not, however, distinguished between galaxies in the magnitude-limited and color-selected samples. This is because aside from the expected lack of blue galaxies in the color-selected sample, the two samples' color distributions are not distinct. The extreme outlying objects in the UVK plane are almost all very red in $V'-K$. Four of these objects correspond to the objects identified in Paper I as having exceptionally red $N-K$, and in the previous section as having large N band κ-corrections. Four of the seven galaxies with $V'-K>3.75$ are highly inclined systems, which indicates that extinction may be the cause for such red colors. This actually is reassuring, since the purpose here is to accurately reproduce galaxy colors as would be observed in the rest-frame, which would include the effects of reddening.

The features of the galaxy locus in the UVK plane that are most striking are the knee at $U-V'=0.7$ and $V'-K=3.3$, the constancy of $V'-K$ for all $U-V'$ redder than this knee, and the extended blue tail above the knee. This blue tail is characterized by rapidly changing and broad range of $V'-K$ over a small interval in $U-V'$. The spectral types change smoothly along the locus, as one would hope given the correlation of Hubble type to color. The typical Hubble type at the knee is Sbc (Aaronson 1978), as reproduced here in Fig. 14. The knee also represents the transition between b-type and a,f,g-type galaxies.

The mean colors of am- and fm-type galaxies are remarkably similar, although not identical. This is true in $U-V'$ and $V'-K$, as seen in Fig. 14, as well as other colors, as listed in Table 4. The comparable mean colors do not neces-

TABLE 4. Average rest-frame colors, errors, and standard deviations by spectral type.

		$U-J$			$J-F$			$F-N$			$N-K$		
Type	N	$\bar{c}$	$\overline{e(c)}$	$\sigma(c)$	$\bar{c}$	$\overline{e(c)}$	$\sigma(c)$	$\bar{c}$	$\overline{e(c)}$	$\sigma(c)$	$\bar{c}$	$\overline{e(c)}$	$\sigma(c)$
bk	34	−0.03	0.05	0.17	0.66	0.05	0.15	0.62	0.08	0.10	1.58	0.15	0.28
bm	22	0.05	0.05	0.13	0.83	0.05	0.14	0.88	0.05	0.09	2.01	0.11	0.19
am	26	0.37	0.06	0.17	0.98	0.05	0.11	0.89	0.06	0.08	1.96	0.10	0.16
fm	34	0.35	0.07	0.17	0.95	0.06	0.15	0.85	0.06	0.09	1.95	0.09	0.18
gm	51	0.62	0.15	0.12	1.07	0.07	0.12	0.89	0.08	0.11	1.96	0.07	0.16

sarily imply that any two am and fm galaxies have the same colors in all bands, but perhaps indicate there are only four distinct spectral types instead of five. However, the stellar fraction, $f_{c,F}$, has different characteristic values and ranges for the two types am and fm; although am- and fm-type galaxy colors are similar, the implied stellar composition is significantly different. As it turns out, we will find other reasons to distinguish between am and fm galaxies later.

Finally, we note that there is some evidence for the bifurcation in the *UVK* color distribution suggested by Aaronson (1978). He observed that if globular clusters were included in the *UVK* plane and considered a low-mass extension of early type systems, such systems formed a separate locus at blue $V-K$ but redder $U-V$ than the late-type galaxies (as reckoned on the Hubble system). A hint of this effect is seen in the distribution of objects redder than $U-V'=1$ in Fig. 13. In addition, the mean fm-type galaxy colors are marginally bluer in $V'-K$ than in $U-V'$ compared to am-type galaxies. More generally, in our spectral classification, the k-type galaxies are uniformly on the blue side of the locus in $V'-K$, while traversing a large range in $U-V'$. This is an interesting clue as to the nature of the dispersion in this diagram, which we discuss in Sec. 5.

4.3.1 The second spectral classification parameter

To give a better sense of what role the second parameter of our spectral classification—namely the stellar fraction—plays in describing the spectral type, we have plotted rest-frame $U-V'$ and $V'-K$ vs $f_{c,F}$ in Fig. 15. Galaxies separate into different loci as a function of spectral type in $U-V'$ vs $f_{c,F}$, and the slope of the correlation becomes steeper as the hot component becomes progressively hotter. Since $U-V'$ is sensitive to the average stellar effective temperature, this steepening is what is expected as the effective temperatures of the hot and cool components become more divergent. This explains, in part why the hotter spectral types have a smaller range of $f_{c,F}$ (Sec. 2.2).

It is interesting to note that the five gm-type galaxies just below the fm locus, which are well separated from the gm locus, have hot stellar components that are on the border between G and F stars. We suspect that the discontinuity between spectral types in this diagram may be due to discontinuities in the stellar library. This is seen more clearly in the correlation of $V'-K$ and $f_{c,F}$. Here, the slope of the correlation between $V'-K$ and $f_{c,F}$ for different spectral types appears to be roughly the same. However, note that there are four clumps of objects, moving from large to small $f_{c,F}$: one composed only of bk- or ak-type galaxies, the second containing bm through gm types, the third containing fm and gm types, and the fourth containing mostly gm types. The galaxies in these clumps are distinguished by their cool stellar components, and the groupings correspond to breaks in the adopted stellar library (refer to Fig. 7): 162–166, 156, 152–153, 135–141, respectively. Inasmuch, the discontinuities are likely to be artificial.

The results that we take away from these diagrams is that for a given spectral type, $f_{c,F}$ correlates with the range of rest-frame color within that spectral class. The strength of the correlation with color depends both on the color (e.g., $U-V'$ or $V'-K$) and the spectral type, and these correlations ideally should change smoothly between spectral types.

5. DISPERSIONS IN GALAXY COLORS: THE COLOR–LUMINOSITY EFFECT

In this section we show that color–luminosity effects are manifest in the *UVK* plane for all galaxy types. Although it

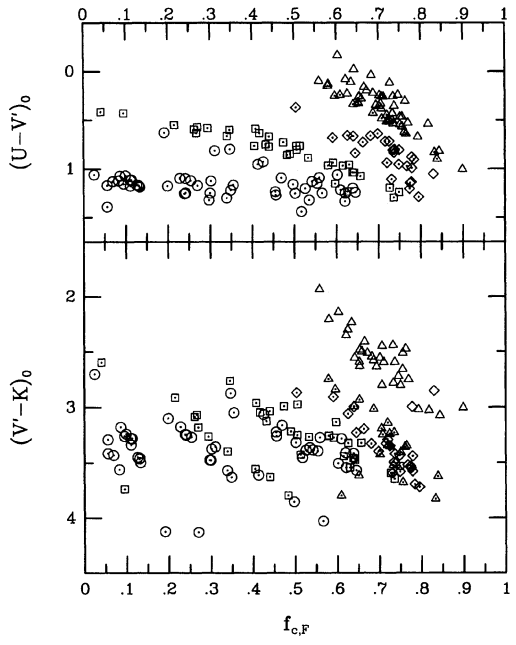

FIG. 15. The distribution of rest-frame $U-V'$ (top panel) and $V'-K$ (bottom panel) colors with stellar fraction, $f_{c,F}$. Objects are marked as in Fig. 8. Galaxies with >20% saturation in any band have been excluded from the plot.

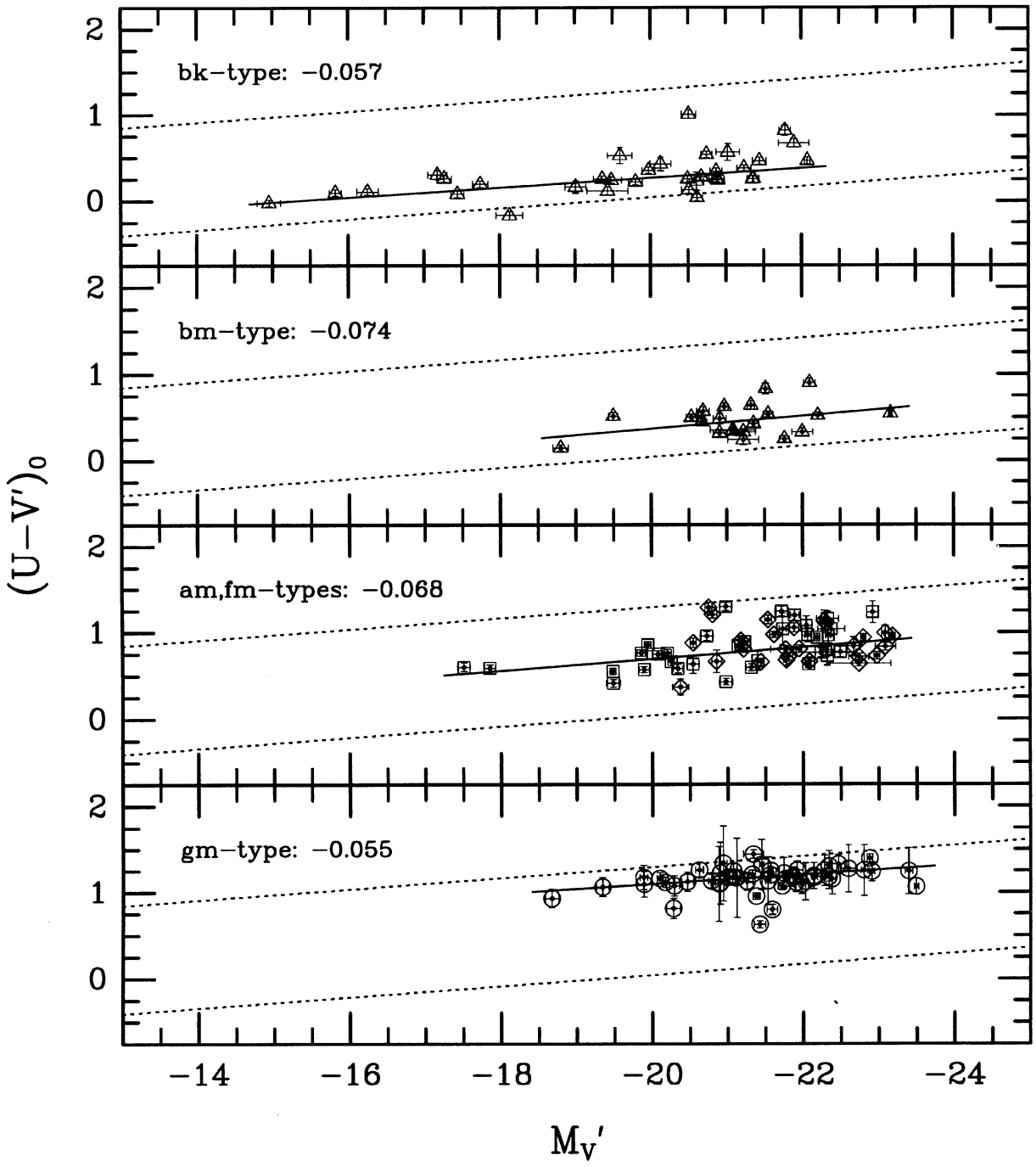

FIG. 16. The color–luminosity effect is shown for each spectral type for rest-frame $U-V'$ vs $M_{V'}$. Linear regressions, described in the text, are shown as solid lines, and their slopes are indicated next to the spectral type. Dotted lines are drawn at a separation of 1.25 mag with slopes equal to the average for all spectral types. The zero-points of these lines are set arbitrarily to bracket the combined distribution of all spectral types. Error bars represent estimated photometric errors.

is difficult to determine, for example, the unique star formation histories of galaxies via the dispersion in $U-V,V-K$ colors alone, our data set can be used to statistically map the correlation of color and luminosity. Such a mapping should provide constraints on models of evolving galaxy populations. Similarly, the roles of various physical mechanisms in producing color–luminosity effects, e.g., age and metallicity, are also not well constrained by observations of colors alone. We suggest that an empirical approach to studying these effects within the framework of our spectral classification is different than viewing these effects within the framework of the Hubble system. In this context, spectral classification

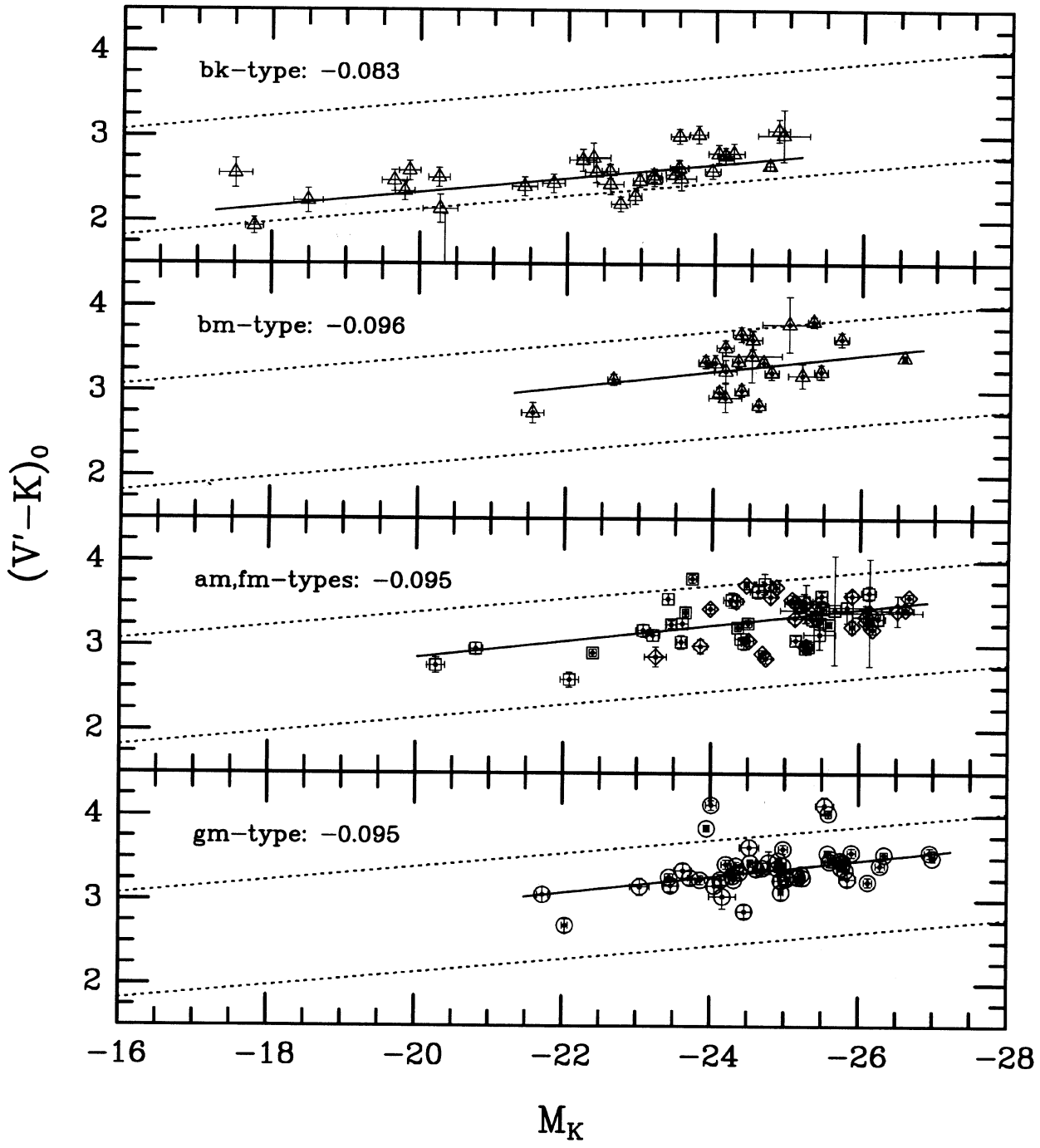

FIG. 17. The same as Fig. 16, except for rest-frame $V'-K$ vs M_K.

may offer new insights on the nature of the relationship between color and luminosity.

5.1 Expectations and Observations

Both the trend and dispersion of galaxy colors in the *UVK* plane contain information about physical parameters that determine these colors. In many regions of the galaxy distribution in Fig. 13, the dispersion is significantly larger than the characteristic errors. The traditional interpretation based on galaxy models (Struck-Marcell & Tinsley 1978; Charlot & Bruzual 1991) is that the shape of the color distribution naturally represents galaxies with different star formation histories. In this picture, the dispersion arises from differences in age or time since the last burst of star forma-

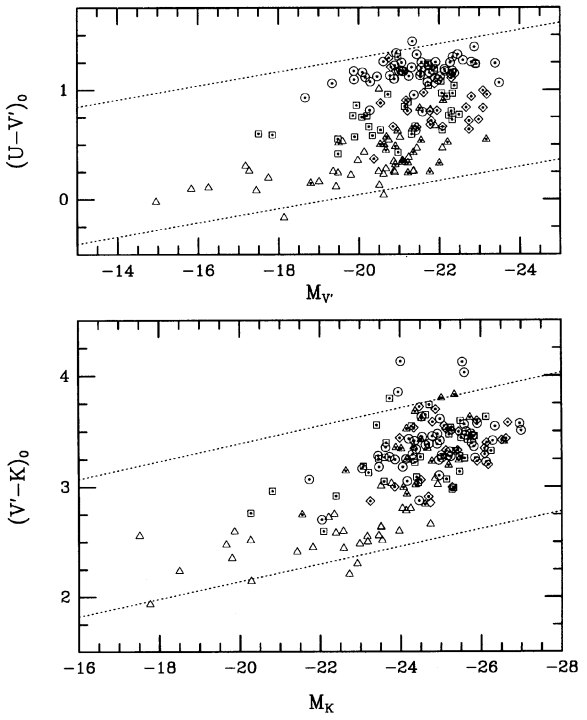

FIG. 18. The color–luminosity effect is shown for all spectral types together for rest-frame $U-V'$ vs $M_{V'}$ (top panel) and rest-frame $V'-K$ vs M_K (bottom panel). Dotted lines are drawn at a separation of 1.25 mag with slope equal to the average for all spectral types. The zero-points of these lines are set arbitrarily to bracket the combined distribution as defined by this figure. Objects are marked as in Fig. 8.

tion. However, Struck-Marcell and Tinsley were quite aware that changes in metallicity could also cause significant changes in the $V-K$ color distribution, based on the work of Strom *et al.* (1976). Although the $V-K$ color–metallicity relation for globular clusters confirmed this basic result (Frogel *et al.* 1980), such a calibration does not exist for a complete sample of galaxies. Thuan (1983) has attempted to derive optical-infrared color–metallicity relationships for a handful of galaxies, but only for extreme populations (blue compact dwarfs, dwarf ellipticals, and dwarf irregulars).

Internal extinction due to dust, which may be well correlated with metallicity, will also cause shifts in the observed color distribution. Unfortunately, such shifts are nearly parallel to those expected from changes in stellar metallicity and age (e.g., Fig. 1 of Struck-Marcell & Tinsley 1978). Actually the situation is more complicated. Traditionally, the effects of dust have been modeled as an intervening screen of absorbing material. However, as discussed extensively by Witt *et al.* (1992), one finds that by including more realistic geometries for the mixture of dust and stars (e.g., Disney *et al.* 1989), as well as scattering (e.g., Bruzual *et al.* 1988), the effects on the observed colors can vary substantially. To determine the effects of dust on observed galaxy colors one would need flux measurements extending to the far-infrared as well as information about the spatial distribution of flux. Such data do not exist for any statistical sample of galaxies. The recent debate on whether spiral disks are optically thick or thin (e.g., Disney *et al.* 1989; Valentijn 1990, Bosma *et al.* 1992, Huizinga & van Albada 1992; Kodaira *et al.* 1992; Peletier & Willner 1992) is but one illustration of our poor understanding of the effects of extinction in galaxies. Inasmuch as galaxies do have dust in varying amounts and relative geometries with respect to our line of sight, we would expect to find a dispersion in galaxy colors. However it is not possible at this time to estimate this dispersion with any reliability. Our approach throughout this work is to analyze the trends and dispersions of the observed colors, corrected only for the effects of redshift. Because the redshift corrections are derived from interpolating between observed band, the rest-frame colors should contain the effects of internal extinction, as mentioned in Sec. *4.3*.

Although we have no hope of separating out the effects of age, metallicity, and extinction on the basis of our broadband colors, we can look for correlations of these colors with other observables in the anticipation that such correlations will provide additional clues about the nature of the color distribution. One such observable is luminosity. In Figs. 16 and 17 we show the correlation between the rest-frame $U-V'$ and $V-K'$ colors with absolute magnitude in the V' and K bands for each spectral type. (For the remainder of this discussion, colors are in the rest frame, and absolute magnitudes are calculated as described in Sec. 4, assuming the Hubble constant $H_0=50$, the deacceleration parameter $q_0=0.1$, and the cosmological constant $\Lambda_0=0$.)

Linear regressions have been fit to the color–absolute-magnitude distribution for each spectral type separately, except for am- and fm-type galaxies, which have been combined. Such a combination is reasonable since these two spectral types have similar colors, and the combination was motivated because am-type galaxies alone have too small a range in luminosity to derive a reliable regression. Regressions for fm-type galaxies alone were very similar to those measured with am and fm types together. The regressions, which have been weighted by the photometric errors, treat the two variables, color and absolute magnitude, symmetrically, in a manner described by Stetson (1989). This type of fitting procedure is often referred to as an "orthogonal regression," e.g., Isobe *et al.* (1990). An iterative rejection algorithm also has been implemented, for which we have chosen to reject objects lying more than five standard deviations (in error-normalized distance) from the best fitting line. This rejection has been used to avoid biasing the fitting procedure by extreme outlying objects which are clearly distinct from the main distribution (e.g., the four very red objects in Fig. 17 for gm-type galaxies). We find that within three iterations all solutions converged. An inspection of Figs. 16 and 17 reveals that the fits are reasonable. The derived slopes are labeled therein.

The two dotted lines that are drawn bracketing each distribution in Figs. 16 and 17 have slopes equal to the average for all spectral types, and have a fixed separation of 1.25 mag. The zero-points for these dotted lines have been artificially adjusted for each color so that the pair of lines are roughly centered on the observed distribution of all galaxies, illustrated in Fig. 18. The purpose of these lines is to show that (1) the slope of the color–luminosity effect is roughly

the same for all galaxy spectral types (quantitatively the slopes have variance of ± 0.009 for $U-V'$ vs $M_{V'}$ and ± 0.006 for $V'-K$ vs M_K); (2) the color–luminosity effect for both $U-V'$ and $V-K$ have roughly comparable slopes (-0.064 vs -0.092, on average); (3) the range of galaxy colors at a fixed absolute magnitude is roughly equal to the change in mean color over the observed range in absolute magnitude. These results are not obviously anticipated by previous work. Before we explain what we believe our results suggest, it is worthwhile to review what is known about color–luminosity effects.

The existence of color–luminosity effects has been known for a long time. In fact, Aaronson (1978) pointed out that this was a likely cause for the dispersion along the galaxy locus in the *UVK* plane. However, his anticipation was that such color–luminosity effects would be present in $U-V$ for elliptical, or the redder galaxies only. This may have been because historically the color–magnitude effect was discovered and first quantified in the optical for elliptical galaxies (Baum 1959; de Vaucouleurs 1961; Sandage 1972; Visvanathan & Sandage 1977). Color–luminosity effects were latter found in the near-infrared by Frogel *et al.* (1978b), also for early-type galaxies, and this work formed the basis for Aaronson's interpretation of the scatter in his *UVK* diagram.

As a consistency check on our regressions, Frogel *et al.* (1978b) derived a slope of -0.06 for $U-V$ vs M_V for E and S0 galaxies, comparable to the value derived by Sandage (1972), and in agreement with our values for all galaxies. This can be compared to more recent results for color–luminosity effects for E and S0 galaxies in Virgo and Coma by Bower *et al.* (1992). They find slopes for $U-V$ vs M_V between -0.074 and -0.095 for different subsets of the data. Both Frogel *et al.* and Bower *et al.* also fit regressions to $V-K$ vs M_V. The sense of the correlation is such that the slope would be steeper if the correlation were measured versus M_K. Consistent with this, both studies found slopes somewhat smaller than what we find for $V'-K$ vs M_K, namely -0.07 (Frogel *et al.*) and between -0.074 and -0.091 (Bower *et al.*). In short, the slopes we have found for all galaxy spectral types are comparable to the range of slopes found in previous studies. However the cited studies have been of only the *earliest* Hubble types.

Color–magnitude effects have been found for early-type spiral galaxies as well. Visvanathan & Griersmith (1977) measured the slope of the correlation in $u-V$ vs M_V to be about -0.13 for early-type spirals. This is somewhat steeper than the slope for ellipticals, but note that their photometry does use the standard U band. In a later paper, Griersmith (1980) measured the slope of the $U-V$ vs M_V to be between -0.03 and -0.15 for different Hubble types from S0 to Sb, with an average slope of -0.097. These slopes also tend to be steeper than for earlier Hubble types, reinforcing the earlier result of Visvanathan & Griersmith (1977). We will return to the issue of steepening slopes with Hubble type in a moment. Here we'd like to call attention to the paucity of studies specifically of the *optical* color–luminosity correlations of galaxies later than Hubble type Sb.

Perhaps part of the reason for the lack of optical color–luminosity studies of late-type galaxies was because strong correlations were not expected. Faber (1973) demonstrated that metallicity correlated with color and luminosity for elliptical galaxies. The optical color–luminosity effect for elliptical galaxies was therefore presumed to be due to changes with metallicity in line blanketing in the atmospheres of giant stars and relatively low-mass main-sequence stars. These stars are observed to be the dominant contributors to the integrated light in systems devoid of significant amounts of star formation. We have already discussed the possible cause for the color–luminosity effect in the near-infrared, although we note line-blanketing may be important here too (Frogel & Whitford 1987). For galaxies with appreciable amounts of star formation, the optical color–luminosity effect is expected to disappear since hot stars are less sensitive to line blanketing, and slight variations in the star-formation rate will swamp such effects in the cooler stars. Support for this theoretical expectation is suggested by the fact that de Vaucouleurs (1977) did not find a correlation of optical color with luminosity for spirals within a given Hubble class. However, Huchra (1977) showed that color–luminosity effects existed for his Markarian galaxy sample, both for $U-B$ and $B-V$ vs M_B. Although this correlation was for the sample as a whole, Huchra's study (see his Fig. 10) points to the possibility that color–luminosity effects in the optical may exist for later-type galaxies as well.

In the early 1980's several authors simultaneously discovered that color–luminosity relationships were present in the optical–near-infrared colors of spiral galaxies (Visvanathan 1981; Wyse 1982; Tully *et al.* 1982). However, the interpretation of this effect for spiral galaxies is not as straightforward as the interpretation of the similar effect for early-type galaxies, as discussed by Bothun *et al.* (1984, see also Bothun *et al.* 1985). For example, based on work referenced above on star clusters, it is likely that there exists a correlation of the near-infrared luminosity with metallicity. Hence for a fixed optical luminosity, an optical–near-infrared color should correlate with metallicity. Yet this interpretation can be turned around: Different optical–infrared colors might signify different ratios of hot, young stars to cool, evolved stars at a constant metallicity. Even this interpretation is dubious, given that we do not necessarily know the luminosity, mass, or age of the individual stars dominating the cool component.

Since we observe a color–luminosity relation in the optical for all galaxy types, and further, the slopes are so similar, if this relation is driven by metallicity, then metallicity must coincidentally affect stars of very different effective temperature qualitatively in the same apparent way. Without being certain of the physical interpretation, there is instead a useful, empirical way to think of color–luminosity effects, namely from the perspective of galaxy luminosity functions. For example, we know galaxies with different optical colors have different characteristic luminosities (Binggeli *et al.* 1988; Shanks 1990). These effects can be seen for galaxy spectral types in the color–luminosity diagrams directly: Only the bluest galaxy spectral types (as defined in *all* colors) are found at the faintest absolute magnitudes, and similarly the reddest spectral types are the brightest. This observation is not tautological because over a significant range of

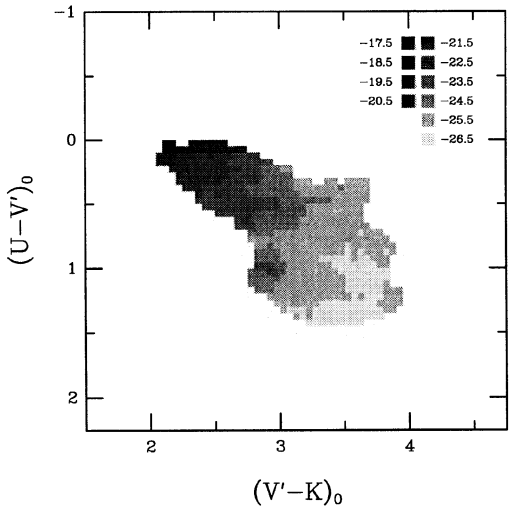

FIG. 19. The distribution of mean K band absolute magnitude as a function of rest-frame $U-V'$ and $V'-K$ color for our galaxy sample (excluding galaxies with >20% saturation in any band). Mean absolute magnitudes were calculated in square bins of color with a width 0.25 mag, sampled every 0.1 mag. Bins with fewer than four objects were not plotted. The range of luminosities is encoded in the greyscale key on the figure. There is a range of 8 mag in mean absolute magnitude across the galaxy locus, or a factor of almost 1600 in K band luminosity.

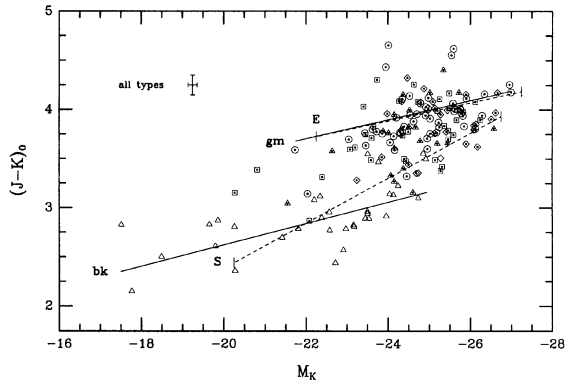

FIG. 20. The color–luminosity effect is shown for our galaxy sample for rest-frame $J-K$ vs M_K, and compared to the mean color–luminosity relations of Mobasher *et al.* (1986) (dashed lines) for ellipticals (E) and spirals (S). Solid lines represent linear regressions to our data for gm and bk types (as described in text). The end-points of all regression lines are defined by the upper and lower limits of luminosity observed in the respective samples. Objects are marked as in Fig. 8, and the characteristic errors are indicated.

absolute magnitude different spectral types coexist, and yet at a given absolute magnitude the different spectral types are separated in mean color. Moreover, galaxy spectral types are not synonymous with "color-classes" defined in a single color. More than one color is involved in the spectral classification, and the spectral types overlap in any given projection onto a subset of the colors, such as $U-V$ and $V-K$. The fact that spectral types overlap more at a given absolute magnitude in the $V'-K$ diagram than in the $U-V'$ diagram is a reflection of the morphology of the UVK plane, namely the degeneracy of $V'-K$ color for a broad range of $U-V'$. Indeed, it is only the bluest galaxies, i.e., bk-type, that are clearly separated in the $V'-K-M_K$ diagram. These are the galaxies in the blue tail of the UVK distribution. In summary, we can view each spectral type as having its own characteristic luminosity and colors as well as a range of colors that correlate with luminosity in a nearly type-independent way.

The fact that both the range of colors at a given absolute magnitude and the slope of the color–luminosity relationship are the same for $U-V'$ and $V'-K$ must be a fortuitous choice of our colors. This becomes clear by inspecting color–luminosity distributions using different bands, as confirmed by other observational studies of field galaxies (e.g., Mobasher *et al.* 1986), as well as theoretical models (Arimoto & Yoshii 1987). However, this does not diminish the fact that correlations with absolute magnitude are as great as the intrinsic dispersion at a given absolute magnitude for $U-V'$ and $V'-K$. Hence any theoretical interpretation of the distribution of galaxies in the UVK plane must take luminosity into account as a fundamental parameter. To this end, we have created a map of the average K band luminosity within the UVK plane in Fig. 19, where the average is representative specifically for our sample and its selection. The map illustrates the smooth trend of luminosity along the galaxy locus, as well as across the locus.

Finally we remark that the am- and fm-type galaxies have average absolute magnitudes that differ by 1 mag, with the am-type galaxies being on average two and a half times more luminous. Thus, although their rest-frame colors are comparable, am- and fm-type galaxies' luminosities are not. Given our sample selection (Paper I), this comparison of characteristic luminosities is fair specifically because am- and fm-type galaxies have similar colors. This difference in characteristic luminosities has led us to retain am and fm types as separate spectral classes.

5.2 *Spectral versus Hubble Classifications*

To explore the spectral type-dependence of the color–luminosity relationship further we again take advantage of the survey of Mobasher *et al.* (1986). Their survey was the first study of optical–infrared color–luminosity effects for a well defined sample of field galaxies. As such, their study provided a systematic investigation of color–luminosity effects as a function of galaxy type and wavelength. Our optical J and K passbands are essentially identical to theirs, and the two surveys are complementary in a number of respects: Although our survey probes about ten times fainter and to redshifts three times larger, their survey benefits from more detailed morphological information. Likewise, although we have four optical and one near-infrared band, they have one optical and three near-infrared bands.

In Fig. 20 we have plotted the (optical) $J-K$ vs M_K color–luminosity diagram for our sample as well as the linear regressions for the Mobasher *et al.* survey ellipticals and spirals, and the linear regressions for gm and bk types. (As with $U-V'$ and $V'-K$, the slopes of the regressions for $J-K$ vs M_K are very similar for all spectral types.) For Mobasher *et al.*'s regressions we have adopted their *explicit* zero-points. Note that both the slope *and* zero-point of

Mobasher *et al.*'s regression for ellipticals is identical to our regression for gm-type galaxies.

We have remarked that there is no strong spectral-type dependence to the *slope* of the color–luminosity relationship. That is, when galaxies of different spectral types are plotted separately, they have the same slope. For this to be true, it requires that we distinguish between bk and bm-type galaxies. This seems reasonable given their distinct distribution in the color–luminosity diagram. However, the slope of Mobasher *et al.*'s regression for spiral galaxies is very different from the slope for elliptical galaxies, and appears to cut across several of our spectral types. We suggest that this disparity may be due to differences in the galaxy classifications used in the two surveys, since Mobasher *et al.* binned their galaxies according to Hubble type. (This same argument can be used to explain the steeping of the optical color–luminosity correlation for spirals, as discussed earlier.) In favor of this suggestion, Mobasher *et al.* find that the residuals of the color–luminosity regression are correlated with residuals of a surface brightness–absolute magnitude regression. Since they assume surface brightness is correlated with disk-to-bulge ratio, this correlation of residuals implies that the disk-to-bulge ratio varies substantially within their bins of Hubble type. Recall that Morgan & Mayall (1957) found that *spectral* type correlated strongly with image concentration, and Kent (1985) in turn demonstrated image concentration correlated strongly with surface brightness. Then we might expect that our spectral classification may well separate galaxies on the basis of their disk-to-bulge ratio. These conjectures may explain the difference between our and Mobasher *et al.*'s interpretation of the "type" dependence of the color–luminosity effect. This will be tested in the future by exploring the distributions of surface brightness and image concentration and their correlation with color for galaxies in our sample.

6. SUMMARY

We have presented a spectral analysis of a statistically complete galaxy sample in order to determine the range and understand better the intrinsic dispersion in galaxy colors. Our analysis has been based on well calibrated *UJFN* photographic photometry and a new *K* band imaging survey of over 170 optically selected field galaxies with spectroscopic redshifts presented in Paper I.

We have argued that the spectral classification of galaxies based on the simplest possible spectral synthesis model is a meaningful approach to the study of distant galaxies. Such a classification is a necessary first step not only to understand the stellar content of galaxies but also to compare meaningfully other observables, such as morphology, at different redshifts. In this context, we have developed a simple spectral synthesis model based on the stellar spectral library of BC93 and have used it to determine what information our broadband colors provide for constraining stellar populations in galaxies. We have found that this library is sufficiently complete to span the observed range of galaxy colors in our sample; that the simple model of Aaronson (1978), which mixes A and M stars is *not* sufficient to fit adequately the observed color distribution; that any *fixed* choice of two stars is likewise inadequate; and that at least four stars are needed in models which fix the set of stellar spectral types. The number of fixed, stellar types needed is equal roughly to the number of colors. We have also found that models which allow both the spectral type as well as the mix to be chosen can fit the observed colors of galaxies with only two or three stellar spectral types. Although we have not developed a formal statistical test to compare our simple models, inspection of the modeled galaxy colors reveals that the two- and three-star models are superior to the fixed four-star model. On the basis of simplicity we have adopted the two-star model. We have proposed that future tests can be made by fitting our simple models to complex synthesis models of known stellar composition.

Our simple spectral classification consists of two spectral labels, b through m, representing the two stellar types (hot and cool) that characterize the broadband colors, and a stellar fraction, $f_{c,F}$, indicating the relative contribution of the two stellar types in the rest-frame F band. Seven distinct galaxy types were found, with 98% of the galaxies belonging to the five types bk, bm, am, fm, and gm. The distribution of spectral types has the following features: (1) the hotter component runs from b though g, whereas the cooler component is only either k or m, with the exception of one galaxy with cool component g; (2) k-type galaxies are essentially all b type; (3) galaxies with the hottest spectral types (b and a) have a very narrow range of stellar fractions, characterized by the value 0.75; (3) cooler galaxies (with the hotter component being f or g) are characterized by a broader range of stellar fractions weighted towards the hotter component; (4) within each spectral type, the stellar fraction correlates with color, most strongly for b and a type and for blue-optical colors. We have compared the stellar fractions found from our simple classification for f- and g-type galaxies to Turnrose's (1976) complex synthesis models of Sc galaxy nuclei. His models show two dominant and distinct spectral types, consistent with our results.

We have described a method for calculating κ-corrections from multiband photometric data with the aid of our simple model, and we have shown that these κ-corrections are reasonable compared to other published results in the optical and near infrared. We have confirmed empirically that the range of κ-corrections for all galaxies in the K band at a given redshift is small (<0.1 mag) out to redshifts of 0.3, and the average K band κ-corrections have been tabulated. The derived κ-corrections for the N and K bands are sensitive to the presence of cool (K and M) dwarfs in the simple model, as are the resulting rest-frame colors. Our results favored excluding cool dwarfs from the models, which is consistent with previous studies which found that cool giants contribute most to the near-infrared light of galaxies (e.g., Frogel *et al.* 1978b).

As a final test of our data and model, we have examined the rest-frame color distribution of our galaxies in the *UBV*, $J_{IR}HK$, and *UVK* planes. We have used our models to derive standard *UBV* and $J_{IR}HK$ colors. The range of rest-frame colors were found to agree remarkably well in the *UBV* plane with Huchra's (1977) local field galaxy sample. Our

rest-frame $J_{IR}HK$ color distribution agrees in the mean with Mobasher *et al.*'s (1986) field galaxy sample, but shows a bifurcation in $H-K$ which appears to be due to the coarseness of the stellar library used for our models. Considering we have no data between N and K, the models simulate remarkably well the mean and range of $J_{IR}-H$ and $H-K$ colors. In the UVK plane we have found the agreement with Aaronson's local galaxy colors, which span all Hubble types, to be excellent. The distribution of spectral types varies smoothly along the Hubble sequence, and our hottest spectral type enjoys a unique location in this diagram that is characterized by blue $V-K$ and $U-V$ colors. Cooler types become increasingly red in $U-V$, but not in $V-K$. Two spectral types, am and fm, have very similar mean rest-frame colors, however their average luminosities differ by almost a magnitude, with the am-type galaxies being more luminous.

To understand further the distribution of galaxies in the UVK plane, we have demonstrated that color–luminosity relationships exists for all spectral types in both $U-V$ vs M_V and $V-K$ vs M_K, over a combined range of 10 mag. The dispersion in color at a given absolute magnitude is comparable to the change in mean color over the observed magnitude range. The color–luminosity effect is not expected to be found in the optical for blue, star-forming galaxies, yet we have found these objects to have the most pronounced effect because of their large range in luminosity. The slopes of the above two color–luminosity relations are very similar, but this result is fortuitous in the sense that other color–luminosity relations (i.e., different bands) have different slopes, as can be confirmed from our data or elsewhere. Given the complexity of inferring the true, underlying, stellar population from galaxy colors, we have refrained from interpreting color–luminosity effects as due to a single, specific mechanism, such as the effects of metallicity on a particular stellar type. Such caution seems particularly prudent since we find color–luminosity effects for galaxies with apparently widely different stellar composition. At some level, color–luminosity effects plausibly represent a connection between galaxy luminosity and star formation history. Therefore any successful model of the color distribution of galaxies in this data set must also be able to match the luminosity distribution.

Finally, we have remarked that the slope of the color–luminosity relationship is similar for all galaxy spectral types in our sample, although the zero-point is type-dependent. We have suggested that the reason why Mobasher *et al.* (1986) find different slopes for different galaxy types is because of the way galaxies have been classified in their study, namely by Hubble type. We have illustrated this for $B-K$ vs M_K, but the same argument may also explain why the slopes for early type spirals in $U-V$ vs M_V are steeper than for ellipticals (Griersmith 1980). This new interpretation was motivated by Mobasher *et al.*'s observation that surface brightness appears to be an additional parameter in color–luminosity relations, plus Morgan & Mayall's (1957) finding that spectral types correlate with image concentration and presumably surface brightness. We will explore this and related issues concerning the connection between galaxy morphology and spectral type in future work.

Note Added in Proof: The optical (J) and near-infrared (K) images of Sa68.10356 in Fig. 16(b) (Plate 22) of Bershody *et al.* (1994, Paper I) are slightly misaligned. The detected source centered in the K image corresponds to the SE object of the pair detected in the J image.

This work is dedicated to my parents and to Amy Stambach. Research was supported by a NASA graduate fellowship (NGT 50677); a NASA Hubble Fellowship (HF-1028.01-92A), from Space Telescope Science Institute, which is operated by the Association of Universities for Research in Astronomy, Incorporated, under Contract No. NAS5-26555; and NSF Grants Nos. AST-87-05517 and AST-88-14251. I have had useful scientific discussions in connection with this work and in Paper I with S. Casey, A. Chokshi, P. Eisenhardt, R. Elston, M. Hereld, C. Graziani, T. Loredo, J. Smetanka, D. Silva, and B. Yanny. None of this work would have been possible without the data set established by R. Kron and D. Koo, which they so generously shared. Most especially, I thank Richard Kron for his help, guidance, and support, and for sharing his boundless inspiration and insight on the nature of distant galaxies.

REFERENCES

Aaronson, M. 1977, Ph.D. thesis, Harvard University
Aaronson, M. 1978, ApJ, 221, L103
Aaronson, M., Cohen, J. G., Mould, J., & Malkan, M. 1978, ApJ, 223, 824
Arimoto, N., & Yoshii, Y. 1986, A&AS, 164, 260
Arimoto, N., & Yoshii, Y. 1987, A&AS, 173, 23
Arimoto, N., Yoshii, Y., & Takahara, F. 1992, A&AS, 253, 21
Baum, W. 1959, PASP, 71, 106
Bershady, M. A., Hereld, M., Kron, R. G., Koo, D. C., Munn, J. A., & Majewski, S. R. 1994, AJ, 108, 870 (Paper I)
Bessell, M. S., & Brett, J. M. 1988, PASP, 100, 1134
Binggeli, B., Sandage, A., & Tammann, G. A. 1988, ARA&A, 26, 509
Bosma, A., Byun, Y., Freeman, K. C., & Athanassoula, E. 1992, ApJ, 400, L21
Bothun, G. D., Mould, J., Schommer, R. A., & Aaronson, M. 1985, ApJ, 291, 586
Bothun, G. D., Romanishin, W., Strom, S. E., & Strom, K. M. 1984, AJ, 89, 1300
Bower, R. G., Lucey, J. R., & Ellis, R. S. 1992, MNRAS, 254, 601
Bruzual, A. G. 1981, Ph.D. thesis, University of California, Berkeley
Bruzual, A. G. 1992, private communication
Bruzual, A., G., & Charlot, S. 1993, ApJ, 405, 538 (BC93)
Bruzual, A., G., Magris, G., & Calvet, N. 1988, ApJ, 333, 673
Buzzoni, A. 1989, ApJS, 71, 817
Charlot, S., & Bruzual, A., G. 1991, ApJ, 367, 126
Coleman, G. D., Wu, C-C., & Weedman, D. W. 1980, ApJS, 43, 393
de Vaucouleurs, G. 1961, ApJS, 5, 233
de Vaucouleurs, G. 1977, The Evolution of Galaxies and Stellar Populations, edited by B. Tinsley and R. Larson (Yale University Press, New Haven)
de Vaucouleurs, G., de Vaucouleurs, A., & Corwin, H. G. 1976, Second Reference Catalogue of Bright Galaxies (University of Texas Press, Austin)

Disney, M., Davies, J., & Phillips, S. 1989, MNRAS, 239, 939
Eisenhardt, P. R. M., & Lebofsky, M. J. 1987, ApJ, 316, 70
Elias, J. H., Frogel, J. A., Matthews, K., & Neugebauer, G. 1982, AJ, 87, 1029
Faber, S. 1973, ApJ, 179, 731
Frogel, J. A. 1985, ApJ, 298, 528
Frogel, J. A. 1988, ARA&A, 26, 51
Frogel, J. A., Persson, S. E., Aaronson, M., Becklin, E. E., Matthews, K., & Neugebauer, G. 1978a, ApJ, 195, L15
Frogel, J. A., Persson, S. E., Aaronson, M., & Matthews, K. 1978b, ApJ, 220, 75
Frogel, J. A., Persson, S. E., & Cohen, J. G. 1980, ApJ, 240, 785
Frogel, J. A., & Whitford, A. E. 1987, ApJ, 320, 199
Glass, I. S. 1984, MNRAS, 211, 461
Griersmith, D. 1980, AJ, 85, 1295
Griersmith, D., Hyland, A. R., & Jones, T. J. 1982, AJ, 87, 1106
Guiderdoni, B., & Rocca-Volmerange, B. 1987, A&AS, 186, 1
Gunn, J. E., & Stryker, L. L. 1983, ApJS, 52, 121
Houk, N., & Fuentes-Williams, T. H. 1982, Michigan Spectral Catalogue (University of Michigan, Ann Arbor)
Hubble, E. P. 1936, The Realm of the Nebulae (Yale University Press, New Haven)
Huchra, J. P. 1977, ApJS, 45, 171
Huizinga, J. E., & van Albada, T. S. 1992, MNRAS, 254, 677
Isobe, T., Feigelson, E. D., Akritas, M. G., & Babu, G. J. 1990, ApJ, 364, 104
Johnson, H. L. 1966, ARA&A, 4, 193
Kennicutt, R. C. 1983, ApJ, 272, 54
Kennicutt, R. C. 1992, ApJ, 388, 310
Kent, S. M. 1985, ApJS, 59, 115
Kodaira, K., Doi, M., & Kazuhiro, S. 1992, AJ, 104, 569
Kron, R. G. 1980, ApJS, 43, 305
Kron, R. G. 1982, Vistas in Astronomy, 26, 37
Larson, R. B., & Tinsley, B. M. 1978, ApJ, 221, 562
Lebofsky, M. J. 1981, ApJ, 245, L59
Lebofsky, M. J., & Rieke, G. H. 1987, in preparation
Lilly, S. J. 1983, Ph.D. thesis, University of Edinburgh, Scotland
Matthews, T. A., & Sandage, A. R. 1963, ApJ, 138, 80
Mazzei, P., Xu, C., & De Zotti, G. 1992, A&AS, 256, 45
Mobasher, B., Ellis, R. S., & Sharples, R. M. 1986, MNRAS, 223, 11
Morgan, W. W. 1970, in Spiral Structure of Our Galaxy, edited by W. Becker and G. Contopoulos (Reidel, Dordrecht)
Morgan, W. W., & Mayall, N. U. 1957, PASP, 69, 291
Oke, J. B., & Sandage, A. 1968, ApJ, 154, 21
O'Connell, R. W. 1976, ApJ, 206, 370
Peletier, R. F., & Willner, S. P. 1992, AJ, 103, 1761
Pence, W. 1976, ApJ, 203, 39
Persson, S. E., Frogel, J. A., & Aaronson, M. 1979, ApJS, 39, 61
Puschell, J. J., Owen, F. N., & Laing, R. A. 1982, ApJ, 257, L57
Renzini, A. 1981, Ann. Phys. Fr., 6, 87
Renzini, A., & Buzzoni, A. 1986, in Spectral Evolution of Galaxies, edited by C. Chiosi and A. Renzini (Reidel, Dordrecht), p. 195
Rocca-Volmerange, B. 1992, in The Stellar Populations of Galaxies, IAU Symposium No. 149, edited by B. Barbuy and A. Renzini (Kluwer, Dordrecht), p. 357
Sandage, A. 1961, The Hubble Atlas of Galaxies (The Carnegie Institution, Washington)
Sandage, A. 1972, ApJ, 173, 485
Sandage, A., & Tammann, G. A. 1981, A Revised Shapley-Ames Catalog of Bright Galaxies (The Carnegie Institution, Washington)
Searle, L., Sargent, W. L., Bagnuolo, W. G. 1973, ApJ, 179, 427
Shanks, T. 1990, in Galactic and Extragalactic Background Radiation: Optical, Ultraviolet, and Infrared Components, IAU Symposium No. 139, edited by S. Bowyer and C. Leinert (Kluwer, Dordrecht), p. 269
Stetson, P. B. 1989, The Techniques of Least Squares and Stellar Photometry With CCDs, a series of five lectures presented at V Escola Avançada de Astrofisca (Dominion Astrophysical Observatory, Victoria)
Strecker, D. W., Erickson, E. F., & Witterborn, F. C. 1979, ApJS, 41, 501
Strom, S. E., Strom, K. M., Goad, J. W., Vrba, F. J., & Rice, W. 1976, ApJ, 204, 52
Struck-Marcell, C., & Tinsley, B. M. 1978, ApJ, 219, 46
Thuan, T. X. 1983, ApJ, 268, 667
Tinsley, B. M. 1980, Fund. of Cosmic Phys. 5, 287
Tully, B., Mould, J., & Aaronson, M. 1982, ApJ, 257, 527
Turnrose, B. E. 1976, ApJ, 210, 33
Valentijn, E. A. 1990, Nature, 346, 153
van den Bergh, S. 1960a, ApJ, 131, 215
van den Bergh, S. 1960b, ApJ, 131, 558
Visvanathan, N., & Griersmith, D. 1977, A&A, 59, 317
Visvanathan, N., & Sandage, A. 1977, ApJ, 216, 214
Visvanathan, N. 1981, A&A, 100, L20
Whitford, A. E. 1971, ApJ, 169, 215
Whitford, A. E. 1975, in Galaxies and the Universe, Vol. 9 of Stars and Stellar Systems, edited by A. Sandage, M. Sandage, and J. Kristian (The University of Chicago Press, London), p. 159
Witt, A. N., Thronson, H. A., & Capuano, Jr., J. A. 1992, ApJ, 393, 611
Woolf, N. J., Schwarzschild, M., & Rose, W. K. 1964, ApJ, 140, 833
Wyse, R. 1982, MNRAS, 199, 1P
Yoshii, Y., & Takahara, F. 1988, ApJ, 326, 1